Estimation of Solanum Tuberosum L. carbon assimilation by the Farquhar model : Evaluation of performance and attempts of improvement for water stress episodes

Auteur : Vanden Brande, Florian
Promoteur(s) : Longdoz, Bernard; Beauclaire, Quentin
Faculté : Gembloux Agro-Bio Tech (GxABT)
Diplôme : Master en bioingénieur : sciences et technologies de l'environnement, à finalité spécialisée
Année académique : 2020-2021
URI/URL : http://hdl.handle.net/2268.2/12249

LIÈGE université
Gembloux
Agro-Bio Tech

Estimation of *Solanum Tuberosum L.* carbon assimilation by the Farquhar model: Evaluation of performance and attempts of improvement for water stress episodes

Vanden Brande Florian

TRAVAIL DE FIN D'ETUDES PRÉSENTÉ EN VUE DE L'OBTENTION DU DIPLÔME DE MASTER BIOINGÉNIEUR EN SCIENCES ET TECHNOLOGIES DE L'ENVIRONNEMENT

ANNÉE ACADEMIQUE 2020 - 2021

PROMOTEURS:
PR. LONGDOZ BERNARD
IR. BEAUCLAIRE QUENTIN

[1] L'autorité académique est représentée par le promoteur, membre du personnel enseignant de GxABT (Bernard Longdoz)

[2] The academic authority is represented by the thesis supervisor, a member of the GxABT teaching staff (Bernard Longdoz)

LIÈGE université
Gembloux
Agro-Bio Tech

Estimation of *Solanum Tuberosum L.* carbon assimilation by the Farquhar model: Evaluation of performance and attempts of improvement for water stress episodes

Vanden Brande Florian

TRAVAIL DE FIN D'ETUDES PRÉSENTÉ EN VUE DE L'OBTENTION DU DIPLÔME DE MASTER BIOINGÉNIEUR EN SCIENCES ET TECHNOLOGIES DE L'ENVIRONNEMENT

ANNÉE ACADEMIQUE 2020 - 2021

PROMOTEURS:
PR. LONGDOZ BERNARD
IR. BEAUCLAIRE QUENTIN

This master's thesis was completed in the Biosystems Dynamics and Exchanges (BIODYNE) department (Gembloux Agro-Bio Tech, University of Liège)

Je voudrais tout d'abord remercier mes promoteurs Quentin Beauclaire et Bernard Longdoz dont la patience et les critiques bienveillantes ont permis à ce travail de voir le jour.

Je tenais aussi à remercier toutes les personnes avec qui j'ai eu l'occasion de travailler au sein de l'équipe Biodyne : Alain Debacq, François Boland, Clément Dumont ainsi que les autres TFistes Clara Cravatte et Matthieu Delespesse pour l'ambiance de travail et la volonté constante de mettre en commun les connaissances acquises. Je remercie particulièrement Laura Delhez qui a passé un temps certain à démystifier TADA et m'a permis de mieux l'appréhender dans toute sa complexité.

Enfin, je tiens à témoigner toute ma reconnaissance à mes parents Xavier et Isabelle, mes grands-parents Christian et Annie, mon frère Adrien, mes cokoteurs et amis Guillaume, Lucas et Julien ainsi qu'à ma copine Justine pour leur soutien inconditionnel et leurs encouragements qui m'ont été d'une grande aide.

Abstract

Mechanistic models of terrestrial ecosystems are our best tools to understand and anticipate the impact of climate change on carbon, water and nutrient cycles. However, many fail to reproduce the decrease in CO_2 assimilation when a prolonged period of edaphic stress occurs. As a consequence of global warming, droughts are expected to increase both in severity and frequency. Therefore, it is essential to understand the processes underlying this phenomenon as well as our current models limitations. The present study attempts to implement two possible areas of improvements. The first one consists in adding a mesophyll conductance (g_m) in the conductance scheme and the second one consists in taking into account the normalized soil water content (REW) as a limiting factor of some biochemical parameters. For this purpose, gas exchange and fluorescence measurements were performed on potato plants (*Solanum Tuberosum L. Agria*) subjected to different soil water content regimes. It was shown that below a specific REW threshold equal to 0.6, $V_{cmax,app}$, $V_{cmax,real}$ (respectively the maximum carboxylation rate of Rubisco when g_m is and is not taking into account) and g_m decreased rapidly. We uncovered highly significant sigmoidal dependency of these parameters with REW. These considerations allowed the implementation of several simulation scenarios. Implementation of g_m and REW limitations successfully improved the results at leaf scale. Nevertheless, when upscaled to the ecosystem, its performances were poorer than the original model, even for severe drought periods. Even if these working hypotheses seem to be refuted at the ecosystem scale, the analysis showed that other uncertainties could be at the origin of these poorer performances. Special care should be paid to stomatal conductance parametrisation, solar radiation absorption models at canopy and leaf scales for future developments. Furthermore, an expression of $J_{max,25°C}$ independent of $V_{cmax,25°C}$ should be considered.

Mechanistic modelling - CO_2 assimilation - Potato - Edaphic stress - Farquhar model - Relative Extractable Water - Mesophyll conductance - Gas exchange measurements - Fluorescence measurements - Carbon cycle - Photosynthesis

Résumé

Les modèles mécanistes des écosystèmes terrestres sont nos meilleurs outils pour comprendre et anticiper l'impact du changement climatique sur les cycles du carbone, de l'eau et des nutriments. Cependant, beaucoup d'entre eux ne parviennent pas à reproduire la diminution de l'assimilation de CO_2 lorsqu'une période prolongée de stress édaphique se produit. Le réchauffement climatique devrait entraîner une augmentation de la gravité et de la fréquence des sécheresses. Il est donc essentiel de comprendre les processus qui sous-tendent ce phénomène ainsi que les limites de nos modèles actuels. La présente étude tente de mettre en œuvre deux domaines d'amélioration possibles. La première consiste à ajouter une conductance mésophyllienne (g_m) dans le schéma de conductance et la seconde consiste à prendre en compte la teneur en eau normalisée du sol (REW) comme facteur limitant de certains paramètres biochimiques. Pour ce faire, des mesures d'échange gazeux et de fluorescence ont été réalisées sur des plants de pomme de terre (*Solanum Tuberosum L. Agria*) soumis à différents niveaux de teneur en eau du sol. Il a été montré qu'en dessous d'un seuil spécifique de REW égal à 0.6, $V_{cmax,app}$, $V_{cmax,rel}$ (respectivement le taux de carboxylation maximal de la Rubisco lorsque g_m est et n'est pas pris en compte) et g_m diminuaient rapidement. Nous avons mis en

évidence une dépendance sigmoïdale hautement significative de ces paramètres avec REW. Ces considérations ont permis la mise en œuvre de plusieurs scénarios de simulation. L'implémentation de $\mathrm{g_m}$ et de la limitation de $\mathrm{V_{cmax,rel}}$ vis à vis de la REW a permis d'améliorer les résultats à l'échelle de la feuille. Néanmoins, lorsqu'il a été transposé à l'échelle de l'écosystème, ses performances ont été moins bonnes que celles du modèle original, même pour les périodes de sécheresse sévère. Même si ces hypothèses de travail semblent être réfutées à l'échelle de l'écosystème, l'analyse a montré que d'autres incertitudes pouvaient être à l'origine de ces moins bonnes performances. Une attention particulière devrait être portée à la paramétrisation de la conductance stomatique, aux modèles d'absorption du rayonnement solaire à l'échelle de la canopée et des feuilles pour les développements futurs. De plus, une expression de $\mathrm{J_{max,25°C}}$ indépendante de $\mathrm{V_{cmax,25°C}}$ devrait être envisagée.

Modèle méchaniste - Assimilation de $\mathrm{CO_2}$ *- Pomme de terre - Stress édaphique - Modèle de Farquhar - Teneur en eau disponible - Conductance mésophyllienne - Mesures d'échange de gaz - Mesures de Fluorescence - Cycle du carbone - Photosynthèse*

Contents

1 Introduction

1.1 Context

Climate change is one of the greatest challenges humanity has ever faced. The anthropogenic CO_2 released into the atmosphere represents the main contribution to radiative forcing (IPCC 2013). The global mean concentration of atmospheric CO_2 has grown at an increasing rate since pre-industrial times. Its concentration has risen from about 280 ppm to over 415 ppm today (NASA 2021) and is expected to reach over 700 ppm by the end of the 21st century (IPCC 2007). Meanwhile, due to the radiative forcing from greenhouse gases, the mean global temperature is expected to increase from 0.3 to 4.8°C compared to the beginning of the 20th century (IPCC 2014). This trend is likely to continue and even accelerate in the next few decades (IPCC 2013). This growth of ambient CO_2 concentration and temperature should increase the rate of photosynthesis and thus the carbon fixation. The total biomass produced by our ecosystems, particularly for plants with a C3 metabolism should naturally grow (Lawlor and Keys 1993; Drake et al. 1997). This 'fertilisation' by carbon dioxide would have acted as negative feedback to mitigate the effects of climate change. Recent studies have proven that this effect was much less significant than expected, as plants being limited in their adaption ability (Geider et al. 2001; Woodward and Lomas 2004; Leakey et al. 2009).

There is a strong interest in studying photosynthesis, as its main terrestrial process leading to primary production and carbon sequestration. The dynamic models that simulate it are, in fact, our best tools for predicting carbon cycle behaviour and the impact of climate change (Sitch et al. 2008; Canadell et al. 2007; Cadule et al. 2010).

Besides, the increase in global temperatures leads to an alteration in precipitation patterns, frequency and types (IPCC 2013, Dore 2005). Droughts are thus expected to occur more frequently and intensively in the coming years (Coumou and Robinson 2013; Christidis and Stott 2014; Trenberth et al. 2014; Vogel et al. 2019) and particularly in northern Europe (Gudmundsson and Seneviratne 2016). During periods of even mild water stress, the net carbon assimilation (A_n) is expected to decrease (Kaiser 1987). Hence, the droughts in 2003 and 2018 reduced A_n of the European ecosystems (Reichstein et al. 2005a; Granier et al. 2007; Smith et al. 2020). Furthermore, for some ecosystems, it led to a shift in ecosystem behaviour from carbon sinks to carbon sources. This aspect of global warming could induce a positive feedback on itself (Reichstein et al. 2013).

Although it seems accepted that edaphic drought is the main factor in the reduction of photosynthesis uptake (Granier et al. 2007; Reichstein et al. 2007), there is still no consensus on how to implement those effects in models (Zhou et al. 2013). Improving the predictive capabilities of the models would make it possible to assess the effects of drought and the positive feedback it generates. In addition, it would provide a more detailed understanding of the mechanisms that make one species more resilient than another for a given specific abiotic condition. Ultimately, this could lead to a change in land use to mitigate the current trend.

1.2 Choice of the model used

Photosynthesis modelling is the cornerstone of carbon cycle models. In this work, the Farquhar et al. 1980 model was used (Farquhar et al. 1980). This model is based on the enzyme kinetics model and simulates photosynthesis for many terrestrial carbon cycle models. It allows the mechanistic simulation of the physiological assimilation in a leaf as a function of temperature, CO_2 concentration in the chloroplast (C_c), and irradiance. This model is based on two limitations related to biochemical processes:

- The carboxylation rate permitted by ribulose 1.5-biphosphate carboxylase oxygenase or Rubisco with $V_{cmax,real}$ being the maximum rate,
- The photosynthetic electron transport rate based on NADPH requirement with J_{max} the maximum rate,

Due to difficulties to estimate C_c, most of the models assume that it is equal to the intra-foliar CO_2 concentration (C_i) much easier to get and compute. In these conditions, the maximum carboxylation rate of the Rubisco enzyme is considered as apparent ($V_{cmax,app}$).

This sub-model requires a framework of other models (irradiance transmission in the canopy, thermal canopy structure, nitrogen distribution and gas transfer represented through a resistance scheme) to upscale results to the ecosystem. At minimum, it is necessary to provide a photosynthetic active radiation (PAR) transmission model giving the quantity absorbed by each leaf and a conductance scheme to deduce intra-foliar concentration (C_i) from atmospheric CO_2 concentration (C_a). It is also possible to determine e temperature for each leaf level by applying a complete energetic balance but most models assume that leaf and air temperature are equal. Details about the model and its implementation are available in section 2.1.

1.3 Regulation of photosynthesis by conductance scheme

The CO_2 transfer from the atmosphere to the chloroplast stroma (see Figure 1) can be divided into two categories of processes. The first category includes processes related to the physical properties of the atmosphere. Atmospheric CO_2 (C_a) is transported by turbulent transport to the boundary layer above the leaf. It then diffuses through the boundary layer to the leaf surface to reach the stomata. The CO_2 concentration is referred as CO_2 at leaf level and noted C_s.

The second category includes processes that depend on the physiology of the plant. They are characterised by a diffusion transport mechanism. The CO_2 diffuses through the stomata into the sub-stomatal cavity. At this point, the CO_2 concentration is defined as intra-foliar concentration (C_i). To reach the stroma of the chloroplasts, the CO_2 must diffuse through several physical barriers:

- gas phase of the intra-cellular spaces;
- cell walls;
- liquid phase within the cells;

To represent these different processes, the widespread resistance analogy is used. A complete representation of this pathway can be obtained by using four resistances in series :

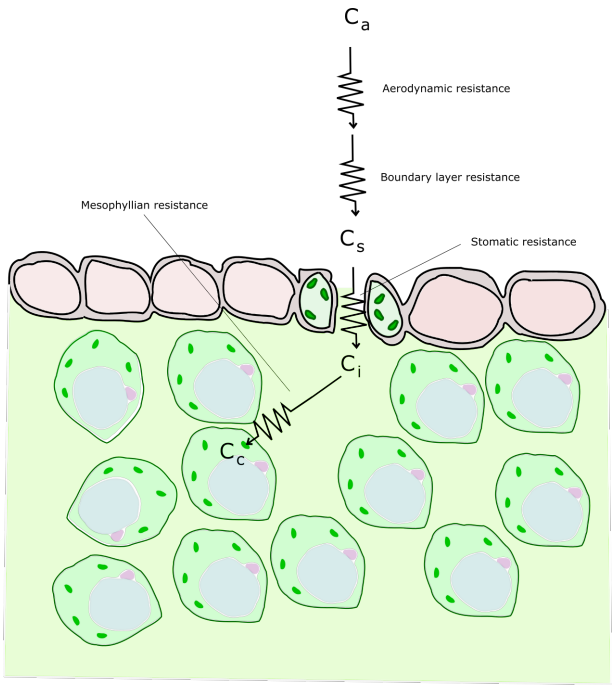

Figure 1: Resistive diagram of CO_2 diffusion from the atmosphere to the chloroplast stroma

- the aerodynamic resistance for the turbulent transfer ($\mathrm{R_{ae}}$)
- the leaf boundary layer resistance for the diffusion through the boundary layer ($\mathrm{R_b}$)
- the stomatal resistance related to the stomatal opening ($\mathrm{R_s}$)
- the mesophyll resistance which summarises the interactions with the three physical barriers defined previously ($\mathrm{R_m}$)

In terrestrial ecosystem models, the concept of conductance is preferred to resistance. It corresponds to the inverse of the resistance and is noted g. The relation between $\mathrm{C_a}$ and the net assimilation ($\mathrm{A_n}$) is expressed with the Fick's law of diffusion :

$$\mathrm{g_{tot}} \cdot (\mathrm{C_c} - \mathrm{C_a}) = \mathrm{A_n} \tag{1}$$

With $\mathrm{g_{tot}}$, the total conductance.

$\mathrm{g_{ae}}$, the aerodynamic conductance, is deduced from transfer of momentum in aerodynamically rough flows (Verma, 1989) :

$$\mathrm{g_{ae}} = \frac{\mathrm{u^{*2}}}{\mathrm{W_{eff}}} \tag{2}$$

$\mathrm{g_b}$, the boundary layer conductance, is defined per square meter of leaf and deduced from an empirical relation assuming a logarithmic wind profile and thus neutral atmospheric conditions (Thom 1972) :

$$\mathrm{g_b} = \frac{\mathrm{u^{*0.67}}}{6.2 \cdot 1.37} \tag{3}$$

With W_{eff}, the horizontal wind speed [m/s], and u^* the friction velocity [m/s] at 2m above the canopy. The 1.37 value is a factor of conversion to switch from water vapour diffusion to CO_2 diffusion (Cowan and Milthorpe 1968).

g_s, the stomatal conductance, is a critical parameter for terrestrial ecosystem models. It influences the incoming diffusion of CO_2 but also the outgoing flow of water vapour through the stomata. Due to its low value, it has a preponderant role compared to the other conductances in the limitation of CO_2 and water vapour fluxes. An increasing g_s coincides with elevating carbon assimilation and water loss through transpiration (E).

Two different approaches exist to simulate the stomatal behaviour: usage of empirical relations and the theory of optimum behaviour.

The first and most widely used approach consists of using empirical observations of stomatal behaviour under specific environmental conditions. It has been proved that g_s depended on photosynthesis, C_a (Wong et al. 1979) and relative humidity (RH) (Ball et al. 1987). It allowed the development of empirical conductance models (Ball et al. 1987; Leuning 1995). As these models are not mechanistic by nature, it is difficult to predict their evolution for different climates or plant functional types (PFT). Therefore, many models using these empiric implementations assume that the parameters are constant for all plants with C3 metabolism (Sitch et al. 2003; Krinner et al. 2005; Law et al. 2006).

The second approach is based on the assumption that the stomata is able to optimize A_n while minimizing E (Cowan and Farquhar 1977). Then the stomata adapt its opening to reduce as far as possible the following variable:

$$\int_{t_1}^{t_2} E(t) - \lambda A_n(t) dt \tag{4}$$

With λ [$molH_2Omol^{-1}C$], a parameter describing the marginal cost of water per carbon gain. Notwithstanding attempts to implement the model (Hari et al. 1986; Lloyd 1991; Katul et al. 2009), it did not initially gain traction given the difficulties in estimating λ and the time step over which it remains constant (Cowan and Farquhar 1977; Thomas and Eamus 1999).

Medlyn et al. 2011 finally demonstrated that the two approaches were in fact compatible. They propose to use relation derivated from the theory of optimum stomatal behaviour with a form similar to empirical relations proposed previously :

$$g_s = g_0 + (1 + \frac{g_1}{\sqrt{VPD}})\frac{A_n}{C_a} \tag{5}$$

VPD is the pressure vapour deficit (Pa). It expresses the atmospheric vapour pressure demand and depends on atmospheric water vapour pressure and leaf temperature. g_1 (-) is a fitted parameter which increases with the ratio E/A_n and the CO_2 compensation point (Medlyn et al. 2011). g_0 corresponds to the conductance remaining in the absence of photosynthetic activity.

This expression of g_s has the advantage of remaining relatively mechanistic (g_1 and g_0 can be related to physical or physiological phenomena) while providing better performance than previously

developed empirical models (Héroult et al. 2013; De Kauwe et al. 2015).

Aside from these two approaches explained above, there is an alternative. It considers the impact of the abscisic acid concentration on the turgidity of guard cells and, by extension, their impact on stomatal opening. It is, in fact, much more mechanical than the theory of optimum behaviour. The problem is that it requires a fine parametrisation, making it impossible to use it on a larger scale than leaf (Dewar 2002).

In addition to atmospheric water demand and $\mathrm{C_a}$, $\mathrm{g_s}$ can be influenced by other physiological factors. Thus, it has been shown that transpiration can be modulated by the hydraulic system (HS) of the plant (Hsiao 1973). When soil water content becomes insufficient to meet the water demand of the atmosphere, stomatal closure can be induced to avoid cavitation within the HS (Jones 1998). A recent study has also shown that $\mathrm{g_s}$ can increase with ambient temperature to surge transpiration and avoid damages to biochemical machinery (Urban et al. 2017).

Several research works have attempted with varying degrees of success to model the impact of water stress on assimilation through a declination of $\mathrm{g_s}$ (Sala and Tenhunen 1996; Wang and Leuning 1998; Kirschbaum 1999; Friend and Kiang 2005). In the Medlyn model, this impact of edaphic stress can be represented by a reduction of $\mathrm{g_1}$ factor when the soil water supply decreases. The relation between $\mathrm{g_1}$ and soil water availability differs widely across climates and PFTs (Zhou et al. 2013; Bonan et al. 2014) and needs to be better understood (Rogers et al. 2017).

$\mathrm{g_m}$, the mesophyll conductance, is considered infinite in most terrestrial ecosystem models. This approximation assumes that $\mathrm{C_i}$ is equal to $\mathrm{C_c}$, neglecting barriers between the stomata and the chloroplast stromata (air, cell walls, lipid membranes and cytoplasm). This assumption also made during the acquisition of parameters necessary to run the model, it results in models encompassing Calvin cycle and $\mathrm{g_m}$ behaviour implicitly.

$\mathrm{g_m}$ is hard to estimate due to the complexity of leaf structure, and when values can be determined, they cannot be easily extrapolated because of the large variability existing between individuals of the same species (Flexas et al. 2012). This lack of knowledge about $\mathrm{g_m}$ is also related to the impossibility to perform direct non-destructive measurements of its value.

Variability of gross primary production (GPP) within a PFT can be greater than between two different PFTs during water stress episodes (Smith et al. 2020). $\mathrm{g_m}$ may be responsible for these substantial divergences in behaviour that can occur within a single PFT (knauer 2016). Many studies conclude that $\mathrm{g_m}$ should no longer be neglected (Kaiser 1987; Walker et al. 2014).

The inclusion of $\mathrm{g_m}$ within the Farquhar et al. 1980 model requires moving from a $\mathrm{V_{cmax,app}}$ representing the mesophyll transfer and the Calvin cycle (where $\mathrm{g_m}$ is an implicit parameter) to $\mathrm{V_{cmax,real}}$ representing only the Calvin cycle with an explicit $\mathrm{g_m}$ value. In this last case, the impact of edaphic water stress can have a repercussion on $\mathrm{V_{cmax,real}}$ and/or on $\mathrm{g_m}$.

1.4 Regulation of photosynthesis by non-stomatal limitation

Recently, numerous studies have questioned the usage of g_s as the sole factor in limiting A_n during water stress events. Several studies put forward the presence of biochemical processes limitations. Generally, these limitations are represented as reductions of $V_{cmax,app}/V_{cmax,real}$ or J_{max} in the Farquhar et al. 1980 model, no matter if this last use the intercellular CO_2 concentration or the chloroplastic one with mesophyll conductance (Krinner et al. 2005; Moorcroft et al. 2001; Sellers et al. 1995).

New research in the field has shown that the exclusive use of stomatal or non-stomatal limitations is not sufficient to explain the behaviour of photosynthesis during a drought event. They suggested that more consistent results could be obtained by including both phenomena (Gourlez de la Motte et al. 2020; Drake et al. 2017; Galmés et al. 2007; Reichstein et al. 2002; Zhou et al. 2013; Perdomo et al. 2017; Keenan et al. 2010). Nevertheless, the contribution of non-stomatal limitations seems to be lower, while their influence is not negligible (Galmés et al. 2007).

Although the impacts of non-stomatal constraints are increasingly documented (Bonan et al. 2014), their modelling needs to be improved (Drake et al. 2017).

1.5 Choice of the potato as study case

Potatoes (*Solanum tuberosum L.*) is the third most-produced crop in the world. In 2019, global potato production exceeded 370 million tonnes (FAOSTAT 2021). In Belgium, in 2019, potatoes were grown on 15% of available arable land. It is one of the highest rates in Europe, behind the Netherlands and Ukraine (FAOSTAT 2021). It is the third most cultivated crop, behind winter wheat (28%) and maise (26%) (STATBEL 2021). It is also one of the most financially profitable, with an estimated income of 4500€/ha ahead of beet (3200€/ha) and grain maise (2800€/ha) (price per ton and yield in 2019, STATBEL 2021).

It is a particularly vulnerable crop to edaphic stress due to its shallow roots (Obidiegwu 2015; Dahal et al. 2019). While, it is an essential crop for developing country where its production has doubled between 1960 and 2005, providing food security, employment and income (Lutaladio and Castaldi 2009). In these countries, rapid population growth and urbanisation associated with climate change create an increased risk of famine (IPCC 2007). Therefore, it is a prime object of study in the context of climate change.

1.6 Scientific issue addressed

The present work aims to determine the best way to account for edaphic stress on A_n estimation. More specifically, the objective is to improve a photosynthesis model for potatoes that meets observations as close as possible by implementing mechanistic functions. The assimilation section of the TADA model already implemented for wheat crops has been used (TADA, Delhez 2019) and calibrated for potatoes. In a first step, the water-stress status will be assessed with a normalised soil water content. The interest of a unique relation between $V_{cmax,app}$ and this water-stress status without taking into account g_m will be evaluated at the leaf scale. The same type of reasoning will be conducted by taking g_m into account and defining the same kind of relation for $V_{cmax,real}$ and g_m.

The most promising model and the original one will be scaled up at plot level and tested using the Lonzée experimental site data. The predicted assimilations will then be compared to the gross primary production obtained with eddy-covariance flux tower measurements performed on the site. We will reference the models as follows:

- M0: Original model, with $\mathrm{V_{cmax,app}}$ only depending on temperature and nitrogen leaf content
- M1: $\mathrm{V_{cmax,app}}$ depending also on temperature and water-stress status
- M2: $\mathrm{V_{cmax,real}}$ and $\mathrm{g_m}$ depending on temperature and water-stress status

2 Material and methods

2.1 Assimilation model description

2.1.1 Leaf scale : Farquhar's equations

The net rate of leaf net assimilation (A_n) is the minimum between photosynthesis limited by electron transport rate (A_j) related to RuBP regeneration and photosynthesis limited by the Rubisco enzyme activity (A_v) minus the day mitochondrial respiration (R_d).

$$A_n = \min(A_j, A_v) - R_d \tag{6}$$

Figure 2 shows how these limitations affect the assimilation for different values of C_i.

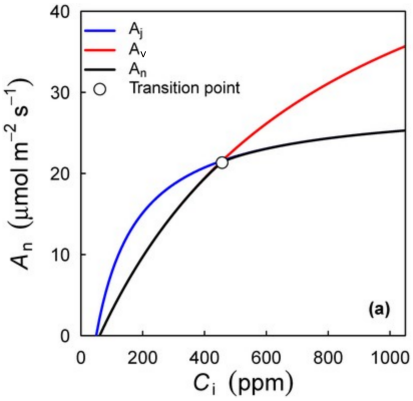

Figure 2: Representation of an A_n-C_i curve with J_{max} and V_{cmax} limitations (Duursma 2015)

A_v is defined with the following expression:

$$A_v = V_{cmax,real} \frac{C_c - \Gamma^*}{C_c + K'} \tag{7}$$

K' is the effective Michaelis-Menten constant of the Rubisco enzyme, and Γ^* is the compensation point of photosynthesis in the absence of mitochondrial respiration. It corresponds to the value of C_c where the flux of CO_2 related to daylight respiration compensates A_n.

K' is given by :

$$K' = K_c \cdot (1 + \frac{O}{K_o}) \tag{8}$$

K_c and K_o are respectively the Michaelis-Menten constants of Rubisco for CO_2 and O_2. O is the oxygen partial pressure in the leaf, considered as constant and equal to 20 500 Pa. V_{cmax}, Γ^*, R_d, K_c and K_o are related to leaf temperature (T, [K]) through the Arrhenius equation (eq. 9). Table 1 resumes values at 25°C and activation energy (E_a) for all photosynthetic parameters proposed in literature.

$$k = k_{25°C} \cdot e^{\frac{E_a \cdot (T - 298.15)}{298.15 \cdot R \cdot (T)}} \tag{9}$$

Where k_T and $k_{25°C}$ are the values of the parameter respectively for a given temperature and at 25°C and R is the gas constant ($8.314 J mol^{-1} K^{-1}$).

	K_c		K_o		Γ^*		R_d		J_{max}		V_{cmax}
	E_a[kJmol^{-1}]	25°C[Pa]	E_a[kJmol^{-1}]	25°C[Pa]	E_a[kJmol^{-1}]	25°C[Pa]	E_a[kJmol^{-1}]	25°C[Pa]	E_a[kJmol^{-1}]	25°C[Pa]	E_a[kJmol^{-1}]
Von Caemmerer et al., 1994	-	40.4	-	24 800	-	3.69	-	-	-	-	-
Badger and Collatz, 1977	59 400	-	36 000	-	-	-	-	-	-	-	64 800
Watanabe et al., 1994	-	-	-	-	-	-	66 400	0.0089 ·$V_{cmax,25°C}$	-	2.1 ·$V_{cmax,25°C}$	-
Farquhar et al., 1980	-	-	-	-	-	-	-	-	37 000	-	-
Jordan and Ogren, 1984	-	-	-	-	29 000	-	-	-	-	-	-
Bernacchi, 2001	79 430	40.28	36 380	27 696	37 830	4.25	-	-	-	-	-
Crous et al., 2013	79 430	40.28	36 380	27 696	20 437	3.87	-	-	-	-	-
Plauborg et al., 2010	-	27.4	-	16 580	-	3.74	-	-	-	-	-

Table 1: Arrhenius parameters (value at 25°C and activation energy) for photosynthesis parameters

The limitation related to J_{max}, A_j, is obtained with the following expression :

$$A_j = J\frac{C_c - \Gamma^*}{4(C_c + 2\Gamma^*)} \tag{10}$$

Where J is the actual rate of electron transport and is obtained by solving the following second-degree equation :

$$\vartheta_l J^2 - (I_{le} + J_{max})J + I_{le}J_{max} = 0 \tag{11}$$

ϑ_l (0.7 [-]) is the leaf response curvature between electron transport and I_{le}, the photosynthetically active radiation (PAR) effectively absorbed by photosystem II (PSII) [$\mu molm^{-2}s^{-1}$]. It depends on incident solar radiation and the spectral correction factor :

$$I_{le} = I_l \cdot \frac{(1 - f)}{2} \tag{12}$$

I_l is the total photosynthetic photon flux density (PPFD) absorbed per unit of leaf area [$\mu molm^{-2}s^{-1}$] and f is the photon fraction absorbed by other elements than PSII (0.15 [-]). At light saturation, the terms including I_{le} in equation 11 become preponderant. We can then neglect ϑJ^2 and the equation becomes :

$$-I_{le} \cdot J + I_{le} \cdot J_{max} = 0 \tag{13}$$

allowing to consider $J = J_{max}$.

J_{max} is determined with the Arrhenius equation modified by Johnson et al. 1942:

$$J_{max} = J_{max,25°C} \cdot e^{\frac{(T-298.15)\cdot E_a}{R\cdot T\cdot 298.15}} \cdot \frac{1 + e^{\frac{S\cdot 298.15 - H}{R\cdot 298.15}}}{1 + e^{\frac{S\cdot T - H}{R\cdot T}}} \tag{14}$$

For energy activation and value at 25°C, are presented in Table 1. $J_{max,25°C}$ is strongly correlated with $V_{cmax,25°C}$ (Walker et al. 2014). Watanabe et al. 1994 proposed to define $J_{max,25°C}$ from $V_{cmax,25°C}$ by multiplying it by a factor equal to 2.1. This factor has been estimated for wheat and has been known to widely vary between different crops (Medlyn et al. 2002). It is therefore necessary to calibrate it for potato crop. S is the temperature response parameter to the electron transport rate, set at $710 Jk^{-1}mol^{-1}$ and H is a curvature parameter (220 000 $Jmol^{-1}$).

To determine $R_{d,25°C}$, the expression developed by Farquhar et al. 1980 has been used :

$$R_{d,25°C} = \frac{\Gamma - \Gamma^*}{\Gamma + K'} \cdot V_{cmax,25°C} \tag{15}$$

Where Γ is the compensation point of CO_2 in the presence of mitochondrial respiration (4.4 Pa, De Pury and Farquhar 1997). This equation can be simplified by considering a linear relation between $V_{cmax,25°C}$ and $R_{d,25°C}$ (Watanabe et al. 1994; De Kauwe et al. 2016).

2.1.2 Canopy scale: De Pury's model

To predict the net assimilation for all leaves within the canopy, it is necessary to apply Farquhar's equations on each leaf by taking into account its exposure, temperature, C_s and VPD and then sum the values. In order to do so, the leaves can either be regarded as similar over the whole canopy (big leaf approach) or can be divided into groups based on similar environmental conditions. In this latter case, the Farquhar et al. 1980 model is applied for one m² of leaf in each group. The results are multiplied by the number of m² of leaf in each class and, finally, summed to obtain the total net assimilation.

In this study, the approach is simplified by considering that leaf temperature, VPD and C_a are identical for all the leaves and equal to the atmospheric values. The only variable input is the PPFD absorbed, depending on the group vertical position in the canopy. The canopy will be divided into infinitely small layers to form the clusters. In each layer, there will be a group corresponding to the sun leaves (which receive direct, diffuse and scattered solar radiation) and another corresponding to the shade leaves (which receive only diffuse and scattered radiation).

The summation over the different groups is done as the sum of 2 integrals representing the sum of the sunlit leaves groups over the different layers and the sum of the shaded leaves over the different layers. There are, therefore, two elements to be determined:

1. the proportions of the leaf area index (LAI) of each layer that is sunny and shaded ;
2. the PPFD absorbed by each of these groups in each layer ;

The first stage is the computation of solar elevation (β) and is explained in Appendix A. Once $\sin(\beta)$ is obtained, the fraction of the surface occupied by sunlit leaf in a layer located in the canopy below a cumulative LAI equal to L is computed by :

$$f_{sun}(L) = e^{-k_b L} \tag{16}$$

where k_b is the extinction coefficient for beam PPFD:

$$k_b = \frac{0.5 \cdot C_l}{\sin(\beta)} \tag{17}$$

With C_l, a clumping factor which can vary between 0 and 1 and describes the trend of the leaf to overlap each other and set to 1 in this case. A clumping factor equal to 1 corresponds to a situation where no overlapping occurs between the leaves inside a layer. The constant multiplying C_l (here equal to 0.5) corresponds to the ratio between the leaf area and its projection on the planar surface perpendicular to the beam solar radiation. When have a spherical distribution, this ratio corresponds to $\frac{\pi \cdot R^2}{2 \cdot \pi \cdot R^2}$ = 0.5.

The PPFD absorbed by the sunlit leaves at canopy depth L corresponds to the sum of a direct-beam ($\mathrm{I_{l,sun}}$), diffuse ($\mathrm{I_{lb}}$) and scattered-beam ($\mathrm{I_{ld}}$) components. Their formulation are presented in Appendix B. Then, the total PPFD absorbed by all the sunlit leaves from the canopy can be obtained by integration along with the L variable:

$$\begin{aligned} \mathrm{I_{sun}} &= \int_0^{\mathrm{L_t}} \mathrm{I_{l,sun}(L)} \cdot \mathrm{f_{sun}(L)dL} \\ &= \int_0^{\mathrm{L_t}} \mathrm{I_{lb}(L)} \cdot \mathrm{f_{sun}(L)dL} + \int_0^{\mathrm{L_t}} \mathrm{I_{ld}(L)} \cdot \mathrm{f_{sun}(L)dL} + \int_0^{\mathrm{L_t}} \mathrm{I_{lbs}(L)} \cdot \mathrm{f_{sun}(L)dL} \end{aligned} \tag{18}$$

Where $\mathrm{L_t}$ is the total LAI for the canopy.

To determine which fraction of PPFD is absorbed by the shaded part of the canopy, we make the difference between the total PPFD potentially absorbable ($\mathrm{I_{tot}}$) and the PPFD absorbed by sunlit leaves. It is expressed as :

$$\mathrm{I_{shaded}} = \mathrm{I_{tot}} - \mathrm{I_{sun}} \tag{19}$$

The detailed expression of $\mathrm{I_{tot}}$ is available in Appendix B.

2.1.3 Relation between $\mathrm{V_{cmax,25°C}}$ and leaf nitrogen content

As explained beforehand, $\mathrm{V_{cmax,25°C}}$ is dependent on the leaf nitrogen content, and, consequently, the nitrogen distribution within the canopy has to be determined. De Pury and Farquhar 1997 used the expression provided by Hirose and Werger 1987 in which the total leaf nitrogen ($\mathrm{mmol_N m_{leaf}^{-2}}$) at canopy depth L is decreasing exponentially with the cumulative relative leaf area index ($\frac{\mathrm{L}}{\mathrm{L_t}}$) from the top of the canopy.

$$\mathrm{N_l} = (\mathrm{N_0} - \mathrm{N_b})\mathrm{e}^{-\mathrm{k_n}\frac{\mathrm{L}}{\mathrm{L_t}}} + \mathrm{N_b} \tag{20}$$

Where $\mathrm{N_0}$, is the total leaf nitrogen content at the top of the canopy, $\mathrm{N_b}$, the fixed part of leaf nitrogen content not associated with photosynthesis and $\mathrm{k_n}$ the coefficient of leaf nitrogen allocation. In this study, we consider that the distribution of nitrogen within the canopy for potato plants is equivalent to that observed for wheat plants. $\mathrm{k_n}$ factor is well determined for wheat and is equal to 0.713 [-] (De Pury and Farquhar 1997).

The relation between nitrogen content related to photosynthesis and $\mathrm{V_{cmax,25°C}}$ is assumed to be linear (Evans 1983; Field and Mooney 1986):

$$\mathrm{V_l} = \mathrm{X_n}(\mathrm{N_l} - \mathrm{N_b}) \tag{21}$$

$\mathrm{V_l}$ is $\mathrm{V_{cmax,25°C}}$ for a given leaf area ($\mathrm{\mu mol_{CO_2} m_{leaf}^{-2} s^{-1}}$) and $\mathrm{X_n}$ is the ratio between $\mathrm{V_{cmax,25°C}}$ and the nitrogen concentration associated to photosynthesis ($\mathrm{\mu mol_{CO_2} mmol_N^{-1} s^{-1}}$).

By integrating $\mathrm{V_l}$ from the top up to the bottom of the canopy and using equations 21 and 20 we can obtain the value of $\mathrm{V_{cmax,25°C}}$ for the entire canopy:

$$V_{cmax,25°C} = \int_0^{L_c} V_l(L)dL = X_n \int_0^{L_c} (N_l - N_b)dL = L_c X_n (N_0 - N_b)\frac{1 - e^{-k_n}}{k_n} \quad (22)$$

The $V_{cmax,25°C}$ of sunlit leaves per ground area can be obtained in the same way by multiplying V_l by the fraction of the surface occupied by sunlit leaves f_{sun} in:

$$V_{cmax,25°C,sun} = \int_0^{L_c} V_l(L) f_{sun}(L)dL = L_c X_n (N_0 - Nb) \cdot \frac{1 - e^{-k_n - k_b L_c}}{k_n + k_b L_c} \quad (23)$$

And thus, $V_{cmax,25°C}$ for shaded leaf fraction can be obtained with :

$$V_{cmax,25°C,shade} = V_{cmax,25°C} - V_{cmax,25°C,sun} \quad (24)$$

With the two leaf classes, A_n becomes:

$$A_n = A_{c,sun} + A_{c,sh} - (R_{d,sun} + R_{d,sh}) \quad (25)$$

2.1.4 Resistance scheme implementation

Along this study, two implementations of resistance scheme will be used. The first is made by using a $V_{cmax,app}$ and C_i concentration to run the Farquhar et al. 1980 model. In this case, the CO_2 pathway can be summarised as a sum of three conductances :

$$g_{tot} = g_{ae} + g_b \cdot L_t + g_s \quad (26)$$

C_i and A_n are two unknowns which are linked together with equation 1:

$$g_{tot} \cdot (C_a - C_i) = A_n \quad (27)$$

To solve the equation and determine both C_i and A_n, the Newton-Raphson algorithm has been used. The resolution is performed twice for respectively sunlit and shaded part of the canopy.

The second uses $V_{cmax,real}$ and C_c and brings into play a slightly modified CO_2 pathway with the addition of g_m in g_{tot} :

$$g_{tot} = g_{ae} + g_b \cdot L_t + g_s + g_m \quad (28)$$

Thus, the equation 26 becomes :

$$g_{tot} \cdot (C_a - C_c) = A_n \quad (29)$$

The A_n - C_c relation is also solved by applying the Newton-Raphson algorithm.

2.2 Plant material and experimental setup (Bordia)

2.2.1 Location and experimental setup

An experimental setup has been realised in a crop field of 4 ha at Gembloux (50°33'47.772" N, 4°42'46.403" E). This plot undergoes intensive crop management involving sugarbeet, potato, wheat and chicory. A 60 m² (12x5m) open-ended tunnel greenhouse was installed near the on-site weather station to simulate drying up episodes. The tarpaulin cover used for the greenhouse is 200 microns thick. Its technical characteristics are described in Table 2.

EVA200i (Ethylene Vinyl Acetate)	
Thickness	200 µm
Transmission rate	90%
Thermicity	80%
Light diffusion rate	90%
UV transmission	70%

Table 2: Technical characteristics of the greenhouse tarpaulin

The area covered by the greenhouse is split into two subplots to reflect two modalities (see Figure 3). In each subplot, 44 tubers from the *Agria* variety were planted in 4 ridges spacing of 60 to 70 cm. Within a row, tubers were spaced 30 to 40 cm apart.

(a)

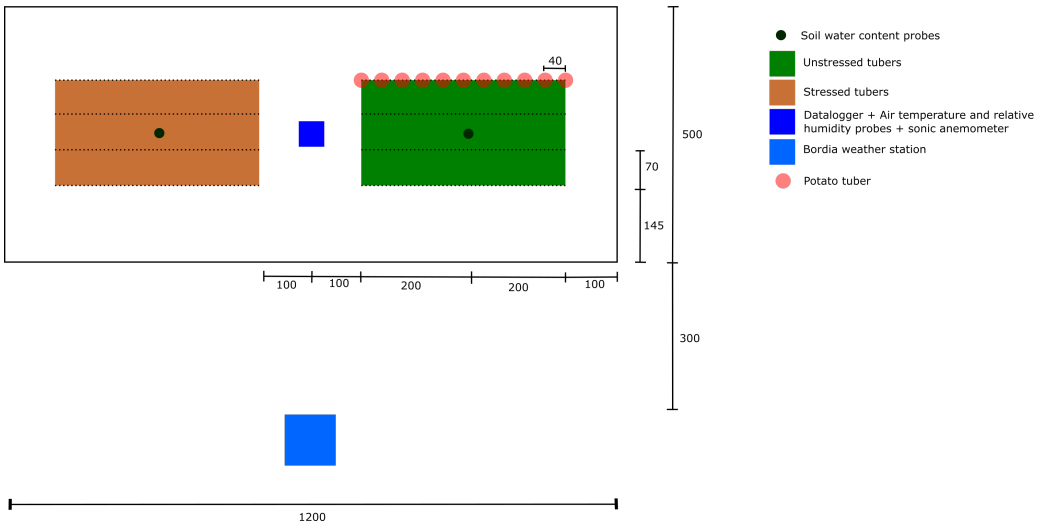

(b)

Figure 3: Bordia setup (a) and experimental diagram (b)

At the centre of each subplot, time domain reflectometers (ML3 Theta Probe, Delta-TDevices, Ltd, Cambridge, UK) were installed at 10, 30 and 60 cm depth to measure soil water content (SWC). A platinum resistance thermometer (PT100D Digital Thermometer MicroStep sport) was installed at 30 cm depth. Under the greenhouse tunnel, air humidity and temperature were measured by a resistor platinum thermometer and electrical capacitive hydrometer (HMP155, Vaisala Oyj, Helsinki, FI) at 1.5 m height. The incident PPFD was also measured with photo-receptor cells (PAR Quantum sens SKP 215, Skye Instruments Limited, Llandrindod Wells, UK).

The tubers were planted on May 15 2020. The first leaves globally emerged from all the tubers on June 5 2020. This date will be referred as the zero of the scale based on "Day after Emergence (DaE)". The experiment ceased on August 20 2020, when the leaves started to show the first signs of senescence. The cultivation period lasted for 77 days (counted from the emergence to the senescence of the crop).

2.2.2 Soil characteristics

Simultaneous measurements of soil water potential and soil water content (SWC, $\mathrm{m}^3_{\mathrm{water}}/\mathrm{m}^3_{\mathrm{soil}}$) were performed on soil sampled at the Bordia experimental field in October 2013. Samples of soil were collected in the 30 first cm of soil and submitted to pressure plate apparatus measurements (Appendix C). These values were used as the basis for calculating the wilting point and field capacity.

The wilting point (WP) is defined as the SWC at which the plant can no longer extract water from the soil. This threshold is determined by the negative logarithm of the water potential (pF). The WP is reached when the matrix potential is equal to -1 580 kPa or pF = 4.2. The field capacity (FC) is the maximum water retention capacity of the soil. It corresponds to the water content of the soil after saturation and 2 to 3 days of drainage (Veihmeyer and Hendrickson 1931). To estimate it, 4 pressure head values (-5, -6, -10 or -33 kPa) can be used (Tóth et al. 2015). To determine which pF corresponds to FC, we cross-checked its value with the determination of an "in situ" FC based on SWC data after 48h of draining. The unstressed plants were watered to saturation at DaE 44, and the soil water content after two days of drainage (DaE 46) was recorded. The result (35.65%) obtained was very close to the SWC with pF = 2.

	SWC [%]
WP (pF = 4.2)	16.2
FC (pF = 2)	35.4

Table 3: Wilting point and field capacity values for Bordia experimental field averaged over the first 30 cm

2.2.3 Drought treatment and REW computation

Unstressed plants were hand-watered during the entire cultivation period to ensure an SWC superior or equal to the field capacity. Each tuber received 1L of water 3 to 4 times a week to maintain the water sensors (10, 30 and 60 cm) above 35% of SWC (Figure 4).

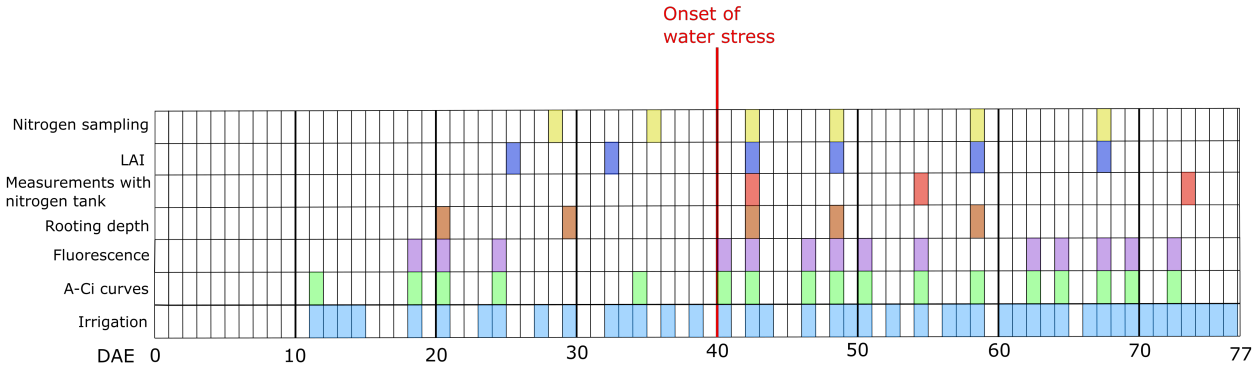

Figure 4: Timeline of Bordia experience

The same treatment has been applied to stressed plants until the end of flowering. It corresponds to the 40th DaE (July 12th 2020, see figure 4). When the daughter tubers started to grow at this stage of development, the watering was stopped. Water stress at this stage usually leads to a significant impact on yields (Deblonde and Ledent 2001).

Drought intensity has been reported by calculating the relative extractable water (REW). It corresponds to the fraction of available water compared to its maximum (corresponding to FC-WP) computed over a layer ranging from the soil surface up to the maximum root depth (Tanner and Ritchie 1974; Granier et al. 1999).

$$\mathrm{REW} = \frac{\int_0^{\mathrm{RD_{max}}} \vartheta(\mathrm{z}) - \vartheta_{\mathrm{WP}}(\mathrm{z})\mathrm{dz}}{\int_0^{\mathrm{RD_{max}}} \vartheta_{\mathrm{FC}}(\mathrm{z}) - \vartheta_{\mathrm{WP}}(\mathrm{z})\mathrm{dz}} \tag{30}$$

Where $\vartheta(\mathrm{z})$ is the SWC at a given soil depth z, ϑ_{WP} and ϑ_{FC} are respectively the wilting point, and the field capacity and $\mathrm{RD_{max}}$ is the maximum root depth. This index varies between 1 and 0 when respectively $\vartheta = \vartheta_{\mathrm{FC}}$ and $\vartheta = \vartheta_{\mathrm{WP}}$ on the entire root depth profile. Values superior to 1 can often be recorded after rainfall or irrigation. For forest, it is assumed that hydric stress on $\mathrm{CO_2}$ fluxes occurs when REW drops below 0.4 (Black 1979; Breda et al. 1995; Granier et al. 1999; Granier et al. 2000; Calvet et al. 2004; Bernier et al. 2006; MacKay et al. 2012). For crops, it is common practice to use a REW threshold of 0.5 (Ding et al. 2013), although values vary significantly between crops. For example, soybeans show signs of water stress only when REW drops below 0.3 (Sinclair et al. 1998), when maize shows signs of water stress at REW = 0.5 (Lei and Yang 2010), and potatoes show a decrease in leaf growth rate at REW = 0.6 (Weisz et al. 1994).

Figure 5 shows the root depth observed during the experiment. It can be seen that from DaE 40 onwards, the root depth starts to stabilise at around 30-35 cm. It turns out that it was also during this period that the stressed plants were no longer watered. Consequently, the soil layer that has to be considered in the REW computation is the ploughed layer, relatively homogeneous. Then, the ϑ_{FC} and ϑ_{WP} were considered as constant in the root depth (values from Table 3) and the integrations in the REW formula were done only on the ϑ variable. Therefore, these integrations correspond to average operations and were realised by computing the mean value of the measurements provided by the 3 probes (10, 30 and 60 cm).

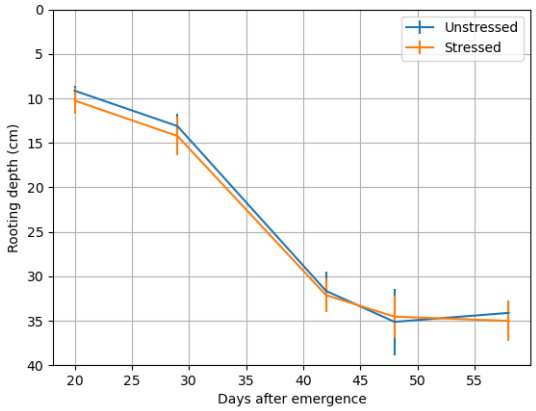

Figure 5: Root depth over time observed at Bordia for stressed and unstressed plants

2.2.4 Leaf nitrogen content measurements

Leaf nitrogen content analyses were performed six times during the experiment (see Figure 4). Three fresh leaves samples were collected at each campaign. They were then placed in an oven for one week at 50°C. Then, they were ground manually to be subjected to a Kjeldahl analysis. Three types of nitrogen are present in leaves: Nitrates, proteic nitrogen and ammonia. The ammoniac fraction is almost negligible, and the Kjeldahl digestion method does not allow to dose of nitrates in the leaves. Usefully, the Kjeldahl analysis results allow the highlighting of dependence between $\mathrm{V_{cmax}}$ and proteic nitrogen.

To convert the fraction of nitrogen in the dry matter (DM, $\mathrm{g_N/100g_{DM}}$) to $\mathrm{mmol_N m^{-2}_{leaf}}$, we use the leaf mass area (LMA, $\mathrm{kg_{DM}/m^2_{leaf}}$). The LMA determination was performed once on July 18 2018, on *Agria* potato leaves using a planimeter and a precision balance. A value of equal to 0.0441 $\mathrm{kg_{DM}/m^2_{leaf}}$ was determined and is assumed to be constant across time.

$$\mathrm{N[mmol/m^2]} = \frac{\mathrm{N[g_N/100g_{DM}]} \cdot 10 \cdot \mathrm{LMA[kg_{DM}/m^2_{leaf}]}}{\mathrm{M_N[g/mol]}} \cdot 1000 \tag{31}$$

2.2.5 Gas exchange measurements: $\mathrm{A_n}$-$\mathrm{C_i}$ curves data set

We carried out joint measurements of $\mathrm{C_i}$ and $\mathrm{A_n}$, the so-called "$\mathrm{A_n}$-$\mathrm{C_i}$ curves" to validate the different hypothesis presented previously. These measurements were performed with the gas exchange device LICOR6400-XT (LI-COR Inc., Lincoln, NE, USA; Figure 6). The principle is to enclose a leaf in a chamber with a light source in which $\mathrm{CO_2}$ and $\mathrm{H_2O}$ concentrations are maintained constant by regulating the incoming $\mathrm{CO_2}$ flux corresponding to the product of the entering airflow (measured with flow-meter) multiplied by its $\mathrm{CO_2}$ concentration (measured with infra-red analyser). The outgoing $\mathrm{CO_2}$ flux is also measured using a flow-meter for the coming out airflow and an infra-red analyser for the $\mathrm{CO_2}$ concentration in the chamber (corresponding to the one going out). The difference between the incoming and outgoing $\mathrm{CO_2}$ fluxes gives the apparent assimilation $\mathrm{A_n}$. The same procedure with $\mathrm{H_2O}$ (also measured with an infra-red analyser) provides the transpiration flux (TR). Knowing water vapour concentration in the inter-cellular space (using leaf temperature measurement and the water

Figure 6: Picture of the LI-6400XT Portable Photosynthesis System

vapour saturation curve) and in the chamber combined with TR allows determining a total water conductance. The contribution of the boundary layer is removed from this total conductance by estimating it with a linear function of the leaf area. The result obtained gives the stomatal conductance for water. Then, we get g_s by dividing this variable by 1.6 (difference in diffusion between CO_2 and H_2O). Finally, C_i is obtained with Fick's law by knowing A_n, C_a and g_s.

Particular attention was paid to the experimental conditions. Indeed, leaf physiology can vary widely with the age of leaf, day time and VPD. Measurements were carried out between 10h AM and 4h PM and on the same leaf class (youngest, most exposed and fully extended leaves). RH and leaf temperature were kept in a range as narrow as possible of the environmental ones, and PPFD was set at 1500 $molm^{-2}s^{-1}$. Which corresponds to the light saturation point ($PPFD_{sat}$, De Kauwe et al. 2016). An acclimatisation time of 20 minutes was observed between chamber closing and each new measurement. It ensures the stability of the carbon dioxide and transpiration flow. Then, A_n was measured in response to 12 values of C_a with the following sequence: 400, 0, 50, 100, 150, 200, 300,400, 600, 900, 1400, 200 ppm. These measurements were performed at 12 dates during the experiment and three times for each date and modality (figure 4).

This dataset will be used to perform the validation of the model at the leaf scale (see summary of data usage in Appendix E). Indeed, the wide range of C_a explored will allow evaluating the capacities of the model to account for the effect that an increase in C_a content could have on the assimilation.

2.2.6 Gas exchange and fluorescence measurements: "one-shot" data set

Fluorescence measurements were carried out before A_n-Ci curves on the same plant and same leaf type with a fluorometer (LICOR6400-40, LI-COR Inc., Lincoln, NE, USA) fixed on the sensor head of LICOR6400-XT. They were performed concomittely with A_n measurements at 12 dates on three plants of each modality on young fully extended leaves to determine $V_{cmax,app}$, J_{max}, g_m, C_c and $V_{cmax,real}$. As for A_n-Ci curves, the relative humidity and the leaf temperature within the measurement cell have been maintained at the same level as environmental ones. During the manipulation, C_a

was set to 400 ppm and PPFD to 1500 $\mu molm^{-2}s^{-1}$ (light saturation condition for photosynthesis). A_n and C_i were recorded (measured in the same way that presented previously), and simultaneously maximum fluorescence (Fm') and steady-state fluorescence (Fs') measurements were performed. By knowing Fm' and Fs', it is possible to get the quantum efficiency of the photosystem II, φ_{PSII} (Genty et al. 1989):

$$\varphi_{PSII} = \frac{F'_m - F'_s}{F'_m} \tag{32}$$

required to determine J_{max} in the Calvin cycle. Since the measurements are taken at light saturation, the approximation can be made that J = J_{max}:

$$J = J_{max} = \alpha \cdot \beta \cdot PPFD_{sat} \cdot \varphi_{PSII} \tag{33}$$

Where α corresponds to the fraction of PPFD absorbed by the leaf and β is the proportion of light absorbed by PSII.

To obtain the product of α and β, Valentini et al. 1995 used the relation between J and the quantum yield of total electron flow φ_{e^-}.

$$J = PPFD_{sat} \cdot \varphi_{e^-} \tag{34}$$

By knowing that 4 electrons are necessary to fix one molecule of CO_2, φ_{e^-} can be derivated from the apparent quantum efficiency of CO_2 uptake :

$$\varphi_{e^-} = 4 \cdot \varphi_{CO_2} \tag{35}$$

This latter is obtained by measuring PPFD, assimilation and respiration under non-photorespiratory condition. It is fulfilled by connecting a tank of N_2 (O_2 concentration < 2 %) to te LICOR6400-XT :

$$\varphi_{CO_2} = \frac{A}{PPFD} \tag{36}$$

where A is the bulk assimilation in the absence of R_d.

By comparing equations 33 and 34 we can see that the $\alpha\beta$ product is actually the slope of the linear regression through the origin between φ_{PSII} and φ_{CO_2} divided by a factor of 4 computed for different PPFD (2000, 1500, 1200, 1000, 800, 600, 400, 200, 100 and 0 $molm^{-2}s^{-1}$).

$$\varphi_{CO_2} = \frac{\alpha\beta}{4} \cdot \varphi_{PSII} \tag{37}$$

The measurement of $\alpha\beta$ was performed at three dates during the experiment (beginning, middle and end of drying episode, see Figure 4) for three different plants of the two modalities. Significant differences have been observed between stressed and unstressed plants ($p < 0.01$) but not across time ($p > 0.05$). For the determination of J_{max}, two values (constants over time) of $\alpha\beta$ have been used: 0.69 ± 0.02 and 0.57 ± 0.04 for respectively unstressed and stressed plants.

Besides, J_{max}, g_m and C_c acquisition, $A_{n,sat}$ and C_i, have been collected to get $V_{cmax,app}$ values, by using the "one-point method" described in De Kauwe et al. 2016. This method assumes that

$V_{cmax,app}$ can be estimated for high irradiation with a single measurement of carbon assimilation at light saturation ($A_{n,sat}$) and C_i (see Section 2.2.5):

$$V_{cmax,app} = \frac{(A_{n,sat} + R_d) \cdot (C_i + K')}{C_i - \Gamma^*} \tag{38}$$

$V_{cmax,real}$ is obtained on the same principle by replacing C_i with C_c :

$$V_{cmax,real} = \frac{(A_{n,sat} + R_d) \cdot (C_c + K')}{C_c - \Gamma^*} \tag{39}$$

This formulation comes from the combination of equations 6 and 7, assuming that under high PPFD, A_n is only limited by V_{cmax}. K' is defined by the equation 8. K_c and K_o necessary to compute as well as Γ^* are derivated from Arrhenius relation (equation 9), Bernacchi et al. 2001 study (cfr. Table 1) and leaf temperature. Since we cannot determine R_d values from gas exchange measurements, two possibilities are available. The first one is to neglect R_d. As we are in conditions of light saturation, at relatively high CO_2 content, A_n will be much more prominent than R_d. The second one, which has been used in this study, is to consider that R_d is equal to 1.5% of $V_{cmax,app}$ or $V_{cmax,real}$ as proposed by De Kauwe et al. 2016 and to introduce this in equations 38 and 39 to have only one unknown (V_{cmax}).

The relation between J_{max} and A_n was used to estimate g_m and C_c (cfr. equations 10 and 6).

$$J_{max} = \frac{(A_{n,sat} + R_d) \cdot (4 \cdot C_c + 8\Gamma_*)}{C_c - \Gamma^*} \tag{40}$$

$$C_c = C_i - \frac{A_{n,sat}}{g_m} \tag{41}$$

By isolating g_m in those equations, we obtain the "variable J method" equation described in Harley 1992 :

$$g_m = \frac{A_{n,sat}}{C_i - \Gamma_* \cdot (\frac{J_{max} + 8 \cdot (A_{n,sat} + R_d)}{J_{max} - 4 \cdot (A_{n,sat} + R_d)})} \tag{42}$$

The large number of parameters determined makes this dataset an ideal base material for model calibration (see data usage in Appendix E).

2.2.7 Normalisation of J_{max}, $V_{c,max,app}$, $V_{c,max,real}$ and g_m

J_{max}, $V_{c,max,app}$, $V_{c,max,real}$ and g_m are assumed to be dependant on leaf temperature. This dependence is often characterised using a simple or a modified Arrhenius equation and needs to be included in M0, M1 and M2 models. Some values already exist in literature for $V_{cmax,app}$ and J_{max}, but they were reassessed for potato. For $V_{cmax,real}$, the same normalisation as the one used for $V_{cmax,app}$ has been assigned, and its robustness has been tested. For g_m, as no dependence on temperature has already been demonstrated, it was decided to test one having the form of a simple Arrhenius function. This part of the analysis was conducted on all values available in the "one-shot" dataset.

For J_{max}, the modified Arrhenius equation has been inverted in order to obtain $J_{max,25°C}$ values. For this purpose, the activation energy determined by Farquhar et al. 1980 has been used (cfr. Table 1). Then, the linear relation between J_{max} and $J_{max,25°C}$ has been assessed. The adjustment is significant on the whole dataset ($p < 0.01$) and for stressed and unstressed plants separately ($p < 0.01$ in both cases) .

For $V_{cmax,real}$, $V_{cmax,apparent}$, the activation energy of Badger and Collatz 1977 was used (cfr. Table 1). As with J_{max}, the quality of the linear regression between $V_{cmax,real}/V_{cmax,app}$ and $V_{cmax,25°C,real}/V_{cmax,25°C,app}$ was assessed. For $V_{cmax,app}$, the fitting was significant for the whole dataset ($p < 0.01$) and also for stressed and unstressed plants ($p < 0.01$ in both cases). The same observation could has been made for $V_{cmax,real}$ with a significant adjustment for the whole dataset ($p < 0.01$) and independently for stressed and unstressed plants ($p < 0.01$ in both cases)

As value at 25°C and activation energy were not available in literature for g_m, the Levenberg-Marquardt algorithm was used to try a fit of the Arrhenius equation on the one-shot dataset. Nevertheless, the regression was not significant ($p > 0.1$). It was therefore considered that no normalisation was necessary for this parameter.

2.3 Relation between REW and biochemical parameters

Since it was expected to get more data in the non-limiting REW range than in the limiting range, we divided the one-shot dataset into REW classes. To do so, we split the dataset in two by considering a pivot point equal to 0.654. A first raw analysis has approximately determined this pivot point. It corresponds to the REW value for a quantile equal to 0.3. Then five quantiles classes were created on either side of this point. In this way, the 30% of data corresponding to plants showing signs of stress have as many points in the regression as the 70% corresponding to unstressed data. Outliers were then removed from $V_{cmax,app}$, $V_{cmax,real}$, J_{max}, A_n and g_m dataset by applying a filter eliminating the values deviating more than 3 times the mean absolute deviation around the median (Leys et al. 2013). It is justified by the fact that LICOR6400-XT measurements can be affected by multiple sources of error (CO_2 leakage, setting of references for H_2O and CO_2 and noise prominence compared to low CO_2 fluxes).

A sigmoid function already widely referenced in literature to describe the influence of different factors on biological phenomena has been used to account for the dependence of the photosynthesis variables ($V_{cmax,25°C,app}$, $V_{cmax,25°C,real}$ and g_m) on REW (Scoffoni et al. 2012):

$$y = \frac{a}{1 + e^{\frac{b-REW}{c}}} \tag{43}$$

y is the dependant variable, a is the asymptote of the sigmoid, b is the REW value when a/2 is reached and c is a curvature parameter.

The fitting was performed on the class means using the Levenberg-Marquardt algorithm with a weight corresponding to the inverse of the variance. Parameters values (a, b and c) and their standard deviation were then deduced.

REW thresholds below which water stress significantly impacts the photosynthesis variables has also been assessed from relation 43. They were defined as the value of REW at which y decreases below a minus its standard deviation:

$$\mathrm{REW_{stress}} = \mathrm{b} - \mathrm{c} \cdot \ln(\frac{\mathrm{a}}{\mathrm{a} - \mathrm{std_a}}) \tag{44}$$

A Monte-Carlo simulation procedure with 10 000 iterations was applied to this relation to determine the uncertainty around $\mathrm{REW_{stress}}$. This procedure used random values of a, b and c in the range of their own standard deviation following a normal distribution.

2.4 Calibration of $\mathrm{J_{max,25°C}/V_{cmax,25°C,app}}$ and $\mathrm{J_{max,25°C}/V_{cmax,25°C,real}}$ ratios

$\mathrm{J_{max,25°C}}$ is strongly correlated to $\mathrm{V_{cmax,25°C}}$ (Walker et al. 2014). In the Farquhar et al. 1980 model, $\mathrm{J_{max,25°C}}$ is defined exclusively from a ratio between the two parameters. This ratio can vary widely between species and climates (Medlyn et al. 2002), and it is essential to calibrate it. However, currently no value of the ratio exists when using $\mathrm{V_{cmax,25°C,real}}$ in model M2.

We grouped data from the one-shot dataset by DaE and by modality to perform the calibration. An orthogonal distance linear regression was performed with the intercept set to 0. During the regression, weights were considered with a value equal to the inverse of the variance for each class. This regression was performed three times: on all data, on data coming from stressed plants and on data coming from unstressed plants. The dataset was split into two groups on both sides of an apparent REW threshold. The threshold corresponds to the one defined in Section 3.1.1. Below 0.6, the measurements are considered as coming from stressed plants. The results are presented in Figure 12.

2.5 Lonzée dataset

In order to evaluate the model's ability to predict assimilations at the scale of an entire ecosystem, it was necessary to use another type of data. The Lonzée Terrestrial Observatory is an experimental crop field of 12 ha located at 3.5km from Gembloux (50°33'5.8"N - 4°44'46.5"E). It is a plot undergoing intensive management for over 80 years with a usual 4-year rotation of beet, winter wheat, potato and winter wheat. It is equipped with an eddy covariance (EC) system measuring net $\mathrm{CO_2}$ and transpiration fluxes exchanged by the ecosystem and a weather station. The EC station of Lonzée is a great tool to perform a wide variety of measurements.

Figure 7: EC acquisition system and weather station in the Lonzée ICOS experimental field

The EC system is composed of a three-dimensional sonic anemometer (Solent Research HS-50, Gill Instruments Lymington, UK) and an infrared gas analyser (LI-7200, LI-COR, Lincoln, NE, US). It measures the wind speed in 3 directions and the concentration of CO_2 and H_2O at very high frequencies (10-20 Hz). The processing of these raw data allows the calculation of net CO_2, water vapour and sensible heat fluxes on a half-hourly basis. This processing is performed using the EddySoft software with the parameters block average and 2D coordination rotation. By convention, the fluxes are negative when they are incoming from the atmosphere to the ecosystem.

To perform the partitioning of the net CO_2 fluxes in its two main components, ecosystem respiration (R_{eco} and gross primary production (GPP = photosynthesis + photorespiration), the REddyProc package available in R language was used (Wutzler et al. 2018). The partitioning is done by separating the data from days and nights. At night, as there is no incident radiation, the only carbon flux is the ecosystem respiration. A relationship is then adjusted to represent the R_{eco} dependence on temperature. During the day, the net CO_2 flux measured (F_C) corresponds to the difference GPP-R_{eco}. Giving that R_{eco} is estimated via relationship defined above and the air temperature, the GPP is obtained by summing F_C and R_{eco} Reichstein et al. 2005b.

The incoming and outgoing radiation in solar and far-infrared domains are performed with a net radiometer (CNR4, Kipp and Zonen, Delft, NL). Incoming and outgoing PPFD data are acquired with photo-receptor cells (PAR Quantum sensor SKP215, Skye Instruments Limited, Llandrindod Welss, UK). Diffuse PPFD measurements are also performed with photo-receptor cells (Sunshine sensor type BF3, Delta-T Devices Ltd, Cambridge, UK). Air temperature and relative humidity are measured at two different heights (2 and 2.9 m) using a resistive platinum thermometer and electrical capacitive hygrometer (HMP155, Vaisala Oyj, Helsinki, FI). In addition, canopy temperature measurements are recorded using an Infra-red Remote Temperature Sensor (Temperature Sensor, IR 120, Campbell, Scientific, Logan, UT, US). The station also collects precipitation data thanks to a weighing gauge rain system (TRwS415, MPS system sro, Bratislava, SK) and atmospheric pressure measurements thanks to the barometer present on site (PTB110/CS106, Campbell Scientific, Logan, UT, US). Temperature and humidity data are also collected at different depths in the soil. We only considered data

returned by the three sensors present in the first 30 cm of depth (-5, -15 and -25 cm). Soil water content is acquired with capacitance sensors (EnviroSCAN Probe, Sentek Sensor Technologies, Step ney, SA, AU) and temperature with platinum resistance thermometers (PT100D Digital Thermometer, MicroStep sport). All the data are acquired once every 10 seconds and averaged on a half-hourly basis.

In 2018, seed potatoes (*Solanum Tuberosum L.*) of the *Agria* variety were grown on the Lonzée plot, and a critical drought phase has been experimented at the end of the cultivating period. For this reason, the same variety was used during the Bordia experimentation. Indeed, it is known that genetic variability existing within *Solanum Tuberosum L.* species could lead to different water usage efficiency (Vos and Groenwold 1989). The upscaling of Bordia results at leaf level to Lonzée ecosystem-level can therefore be made without the risk of bias related to this fact.

During the 2018 season, the leaf area index (LAI) was measured six times, the LMA once, the above-ground biomass estimated six times, the leaf and stem nitrogen content once, and the number of plants per hectare at the beginning of the growing season.

REW values have been computed following the same procedure as the one used for Bordia (cfr. Section 2.2.3). The water content and soil hydraulic potential values were measured on 3 Lonzée soil samples using Richards pressure plate apparatus (Richards, 1943). The results are available in Appendix C. As previously described in Section 2.2.2, a value of $\mathrm{pF} = 2$ was used to define field capacity, which corresponds to an SWC of 36.3 %. This value was confirmed by the moisture content observed at Lonzée 48h after the heavy rainfall of May 1 2018. From April 29 2018 to May 1 2018, 39.5 mm fell. This significant rainfall increased the soil water content of the 0-30 cm soil layer up to 40%. The water content reported 48h after this peak of SWC (May 3 2018) was 34%.

The WP value was defined as the SWC value obtained with the Richards pressure plates when pF was equal to 4.2. These FC and WP values are relatively similar to the Bordia one (16.2%, 35.4%). It is consistent with the fact that the Lonzée and Bordia soils are relatively similar in terms of grain size and organic matter content (Appendix D).

	SWC [%]
WP (pF = 4.2)	16.1
FC (pF = 2)	36.3

Table 4: Values of wilting point and field capacity for the 0-30 cm soil layer at the Lonzée EC station

3 Results

3.1 Leaf scale

3.1.1 REW and biochemical limitations

$V_{cmax,25°C,app}$, $V_{cmax,25°C,real}$ and g_m data dynamics with REW and their sigmoidal fitting are reported respectively in Figures 8, 9 and 10. The p-values (cfr. Tables 5, 6 and 7) prove that the sigmoidal model is highly significant in each case as well as the asymptotes (a) and the mid-slope value (b). However, the curvature factor (c) was non significant for each biochemical parameter considered. It suggests that the data collected are not suffisants to define correctly the form of the transitions between the two asymptotes and the slope. Based ont the r² values of the regressoin presented, the temporal variability of $V_{cmax,25°C,app}$, $V_{cmax,25°C,real}$ and g_m is explained respectively at 91, 66 and 68 % by the REW proving that this variable is the most influencing one. A great variability of the raw values on both sides of the plateau can be noticed for $V_{cmax,25°C,app}$ and $V_{cmax,25°C,real}$. $V_{cmax,25°C,real}$ (Figure 9) fitting show a lower R² value compared to $V_{cmax,25°C,app}$ and the plateau value is twice as high. For g_m, an increase of raw data can be observed after the second plateau (REW > 0.6) when REW reach a value of 0.9.

We can also notice that, in each, when the REW approaches 0.2 in both cases, the curves present a second asymptote very close to 0. In case of severe drought, we will thus observe a stop of the Calvin-Benson cycle because of the carboxylation rate of Rubisco and a g_m tending towards 0.

REW thresholds at which biochemical parameters start to decrease significantly are reported in Figure 11. No significant differences between these thresholds have been identified. It suggests that the first impacts of water stress are undergone at the same time at a REW comprise between 0.53 and 0.6.

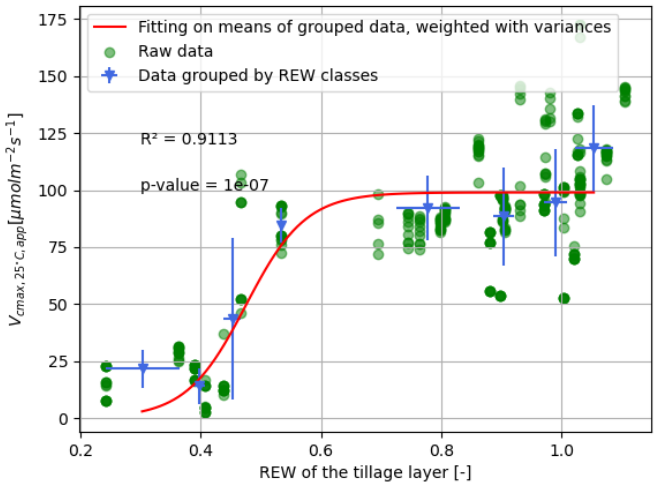

Figure 8: Fitting of the sigmoïd on $V_{cmax,25°C,app}$ and REW data

	Value	p-value
a	98.96 ± 18.41	$p < 0.01$
b	0.4750 ± 0.0406	$p < 0.01$
c	0.0497 ± 0.0222	$p > 0.05$

Table 5: Parameters of the sigmoid highlighting the relation between REW and $V_{cmax,25°C,apparent}$

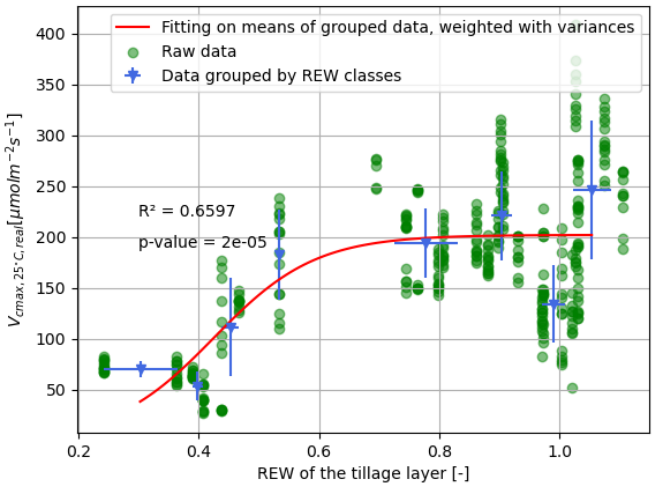

Figure 9: Fitting of the sigmoïd on $V_{cmax,25°C,real}$ and REW data

	Value	p-value
a	202.7 ± 23.09	$p < 0.01$
b	0.4254 ± 0.0502	$p < 0.01$
c	0.0844 ± 0.0576	$p > 0.1$

Table 6: Parameters of the sigmoid highlighting the relation between REW and $V_{cmax,25°C,real}$

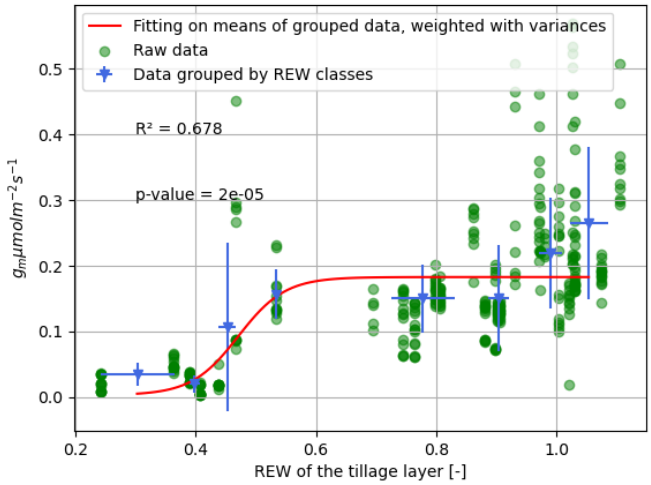

Figure 10: Fitting of the sigmoïd on g_m and REW data

	Value	p-value
a	0.1799 ± 0.0353	$p < 0.01$
b	0.4710 ± 0.0420	$p < 0.01$
c	0.0389 ± 0.0200	$p > 0.05$

Table 7: Parameters of the sigmoid highlighting the relation between REW and g_m

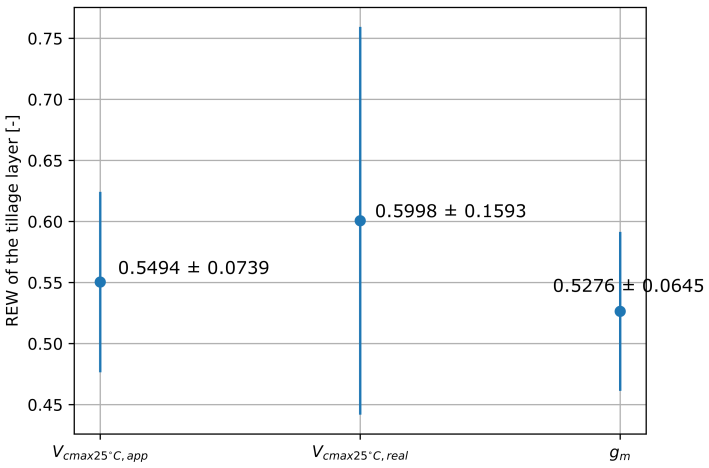

Figure 11: REW thresholds at which a significant decrease of the value of the biochemical parameter is observed based on sigmoïd regressions

3.1.2 $J_{max,25°C}/V_{cmax,25°C,app}$ and $J_{max,25°C}/V_{cmax,25°C,real}$

These ratios have been deduced from experimental data to obtain $J_{max,25°C}$ from the different $V_{cmax,25°C}$ and then to run the models (M0, M1 and M2) at the leaf and ecosystem scale. They have been determined using $V_{cmax,real}$ and $V_{cmax,app}$ and for two ranges of REW (below and above 0.6) corresponding to stressed and unstressed plants. The regression between $J_{max,25°C}$ and $V_{cmax,25°C}$ are presenting in Figure 12 and the slopes and statistics of these regressions in Table 8.

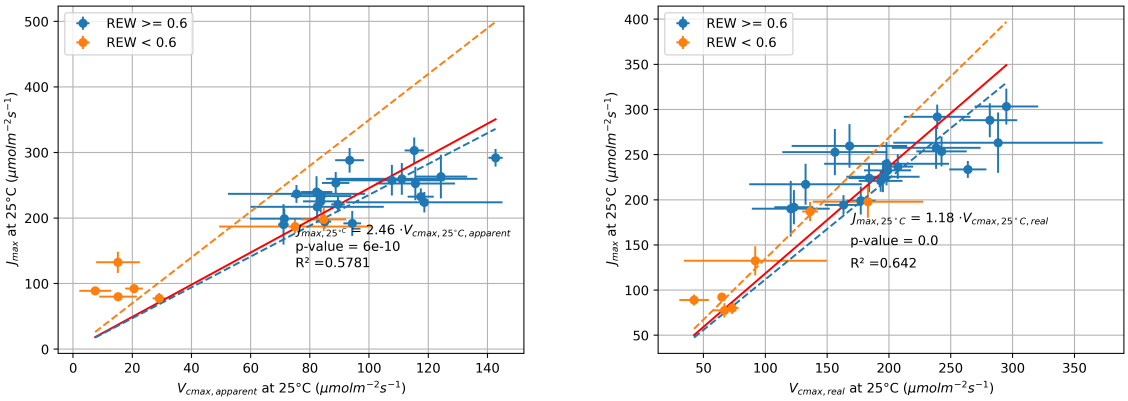

(a) (b)

Figure 12: Ratios $J_{max,25°C}/V_{cmax,25°C,app}$ (a) and $J_{max,25°C}/V_{cmax,25°C,real}$ (b)

		Slope	Standard deviation	p-value
$J_{max,25°C}/V_{cmax,25°C,app}$	**REW < 0.6**	3.497	0.5736	$p > 0.1$
	REW ≥ 0.6	2.354	0.0770	$p < 0.01$
	Overall	2.456	0.1032	$p< 0.01$
$J_{max,25°C}/V_{cmax,25°C,real}$	**REW < 0.6**	1.117	0.0359	$p < 0.01$
	REW ≥ 0.6	1.356	0.0712	$p < 0.01$
	Overall	1.346	0.0380	$p < 0.01$

Table 8: Slopes and statistics of $J_{max,25°C}/V_{cmax,25°C,app}$ and $J_{max,25°C}/V_{cmax,25°C,real}$ regressions

In both cases, the regressions on all data were highly significant. The smaller slope for $V_{cmax,25°C,real}$ case compared to the $V_{cmax,25°C,app}$ one is rather logical because of the larger variability of $V_{cmax,25oC,real}$ as noted above for situations with similar $J_{max,25°C}$ (the presence of g_m in the resistance scheme does not directly impact $J_{max,25°C}$).

It can be seen that for $V_{cmax,25°C,real}$, the three linear regressions are significant. The slopes of the stressed situation are different from the unstressed one, but both slopes show no difference from the slope calculated on all points. By contrast, for $V_{cmax,25°C,app}$ the linear regression for the stressed case is not significant (probably due to the small number of data points). The slope for the unstressed situation is equivalent to the one obtained with all the points.

3.1.3 Nitrogen leaf content

The evolution of the nitrogen content of the most exposed leaves as a function of the days after emergence is reported in Figure 13. Each value corresponds to the average of the three samples used for the analysis, except for the first one, for which only one sample was taken for stressed and unstressed plants.

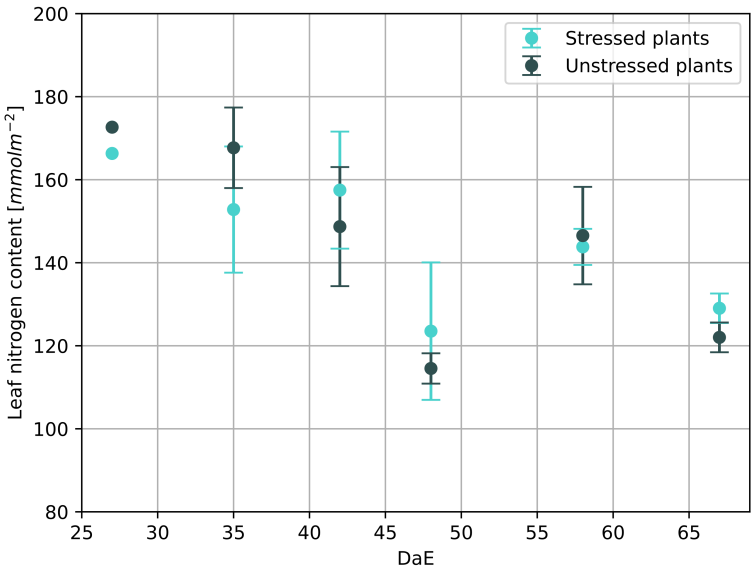

Figure 13: Evolution of nitrogen leaf content of sunny fully extended leaves across time

Leaves showed a highly significant decrease in nitrogen content between the vegetative (DaE 25) and the reproductive stages (DaE 65) ($p < 0.01$). By contrast, no significant difference in nitrogen content could be found between stressed and unstressed plants ($p > 0.1$).

Relations between N and $V_{cmax,25°C,app}$ and $V_{cmax,25°C,real}$ are reported in Figure 14. Linear regression has been performed with the intercept set to 0. The aim was to verify and calibrate the linear relation that is usually used to define $V_{cmax,25°C}$ (cfr. equation 21).

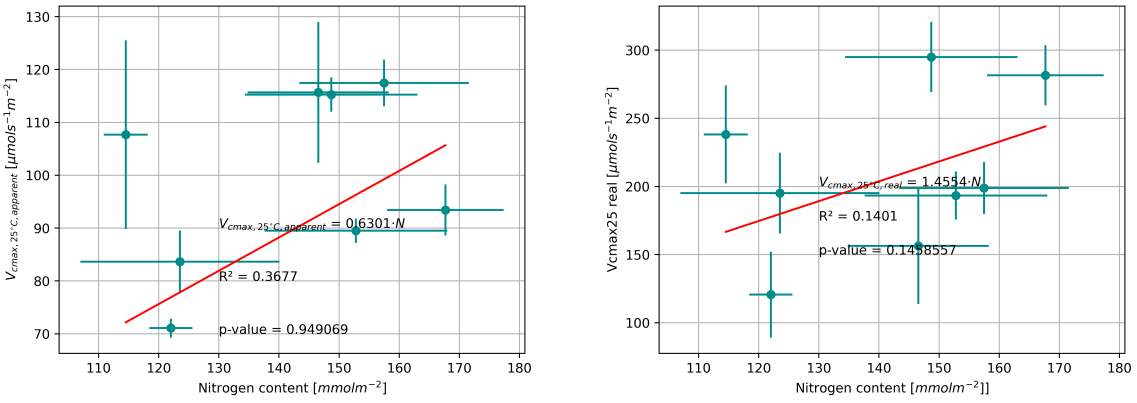

(a) (b)

Figure 14: Relationships between $V_{cmax,25°C,app}$ (a) / $V_{cmax,25°C,real}$ (b) and N (data in blue, linear regression in red)

Nevertheless, no significant linear regression has been found for both $V_{cmax,25°C,app}$ and $V_{cmax,25°,real}$.

3.1.4 Model performances at leaf scale

The first stage in the modelling approach was made at the leaf scale. For this purpose, leaf temperature, C_i and PPFD data from the A_n-C_i curves were used as inputs. A_n was predicted by the model and then compared to the observed assimilation from the A_n-C_i curves dataset. Only two modelling scenarios were evaluated in this case:

- M1 : $V_{cmax,25°C,app}$ defined with the sigmoid dependent on REW (Figure 8)
- M2 : $V_{cmax,25°C,real}$ and g_m defined with sigmoids dependent on REW (Figures 9 and 10)

Values of assimilation at C_a equal to 400 ppm for the A_n-C_i curves dataset, and values of one-shot datasets acquired at the same level of C_a on equivalent leaves from the same plant were compared. Significant differences in assimilation were observed for several dates. As the acquisition conditions are pretty identical in both cases, it is not easy to point to a methodological cause. The only likely reason is a difference in physiology between leaves belonging to the same plant. Therefore, it was decided to exclude A_n-C_i curves when the assimilation at 400 ppm observed was superior to three times the standard deviation plus the mean of the values from one-shot measurements obtained on the same plants. This retrain concerned 7 curves out of 66.

Another problem occurred when testing the model on the A_n-Ci curves. When C_i is low, the assimilation is limited by J_{max} (Figure 2). As shown in Equation 10, if C_i decreases below the Γ^*, the resulting assimilation will show a negative value. As our model does not perfectly define Γ^* due to the lack of a proper calibration for the parameter, this part of the curves was poorly simulated. Since plants never experience these C_i ranges during their growth, data with a C_i value below Γ^* were not kept.

Table 9 summarises the constants used for the different runs of the model (valid also for the runs at the canopy scale).

Γ	4.4 [Pa]
$\Gamma^*_{E_a}$	37 830 [$kJmol^{-1}$]
$\Gamma^*_{25°C}$	4.25 [Pa]
ϑ_J	0.7 [-]
K_{c,E_a}	79 430 [$kJmol^{-1}$]
$K_{c,25°C}$	40.28 [Pa]
K_{o,E_a}	36 380 [$kJmol^{-1}$]
$K_{o,25°C}$	27 696 [Pa]
V_{cmax,E_a}	64 800 [$kJmol^{-1}$]
J_{max,E_a}	37 000 [$kJmol^{-1}$]
R_{d,E_a}	66 400 [$kJmol^{-1}$]
$J_{max,25°C}/V_{cmax,25°C,apparent}$	2.46 [-]
$J_{max,25°C}/V_{cmax,25°C,real}$	1.18 [-]

Table 9: Summary of constants used for leaf and ecosystem scale assimilation simulations

Figure 15 shows the scatterplots of the predicted assimilation versus the measured one. In addition, a colourmap with the REW values was also added to the points.

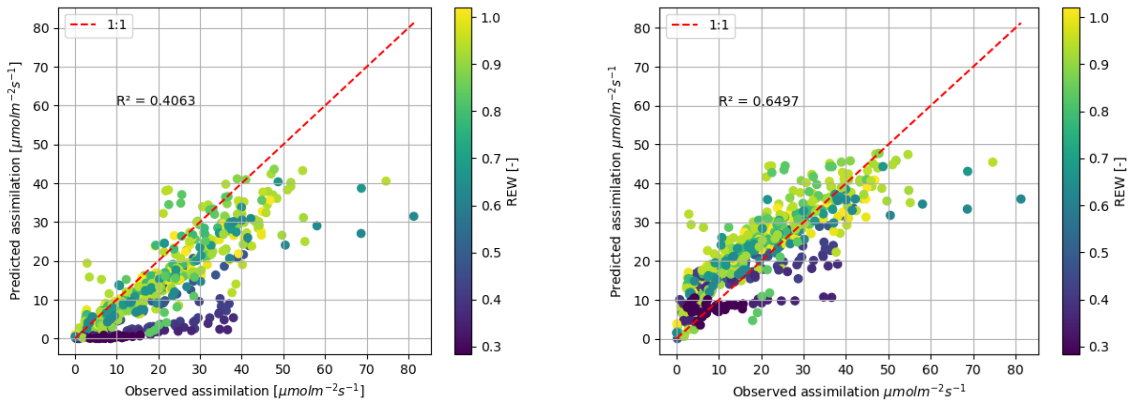

(a) (b)

Figure 15: Scatter plot (assimilation predicted against measured) of the model M1 with $V_{cmax,25°C,app}$ depending on REW (a) and M2 with $V_{cmax,25°C,real}$ and g_m depending on REW (b)

The M2 model showed a better determination coefficient than M1. For model M1, most of the data points are below the bisector. The predicted assimilations are consistently lower than the observed ones.

The model M2 seems to slightly overestimate the assimilations because most points are above the bisector. The graph shows a bi-linear behaviour with a high slope (well above the bisector) between 0 and 5 $\mu molm^{-2}s^{-1}$. Above this breakpoint, the predicted assimilations overestimate the observed assimilations but gradually approach them.

3.2 Ecosystem scale

3.2.1 Inputs required for the model

The purpose of this upscaling is to compare the original version of the model ($V_{cmax,25°C,app}$ dependent only on N (M0), not on REW) with the best of both developed on leaf scale (M2). The upscaling from the leaf to the ecosystem needs additional inputs. In addition to temperature and REW already used at leaf scale, the model requires continuous functions of LAI and N at the top of the canopy as well as g_1 parametrisation for the Medlyn et al. 2011 g_s expression.

The LAI acquired during the 2018 crop in Lonzée (collected 6 times) were related to the growing degree days (GDD), calculated from the values of the weather station of Lonzée via the following formula:

$$GDD = \sum \max(\frac{T_{max} + T_{min}}{2} - T_{base}, 0) \tag{45}$$

Where T_{max} and T_{min} are respectively the maximum and the minimum daily temperature. T_{base} is the minimum temperature required for plant growth. A potato specific value of 7°C was used in this case (Grigorieva et al. 2010).

A second-degree interpolation between the data points was used (see Figure 16) to obtain a continuous function.

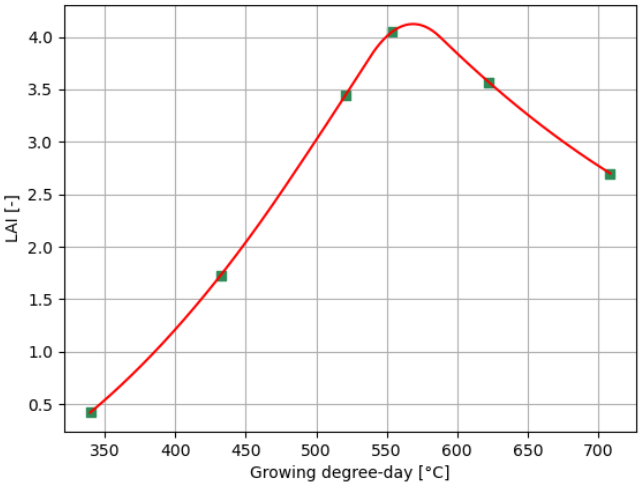

Figure 16: Evolution as a function of GDD at Lonzée in 2018 and interpolation of LAI

The determination of g_1 parameter, needed to compute g_s (cfr. Figure 5) has been performed at the ecosystem scale from EC measurements during a previous study (Beauclaire, personal communi-

cation). This study showed that the dependence of g_1 on REW follows a bilinear function. For the low REW, this dependence follows a decreasing line with a slope equal to -2.97 ± 0.93 ($p < 0.01$) and an intercept equal to 4.10 ± 2.08 ($p < 0.01$) (see Figure 17). A plateau is then observed when the REW is superior to 0.57. This plateau has a value of 2.42 ± 0.05 ($p < 0.01$).

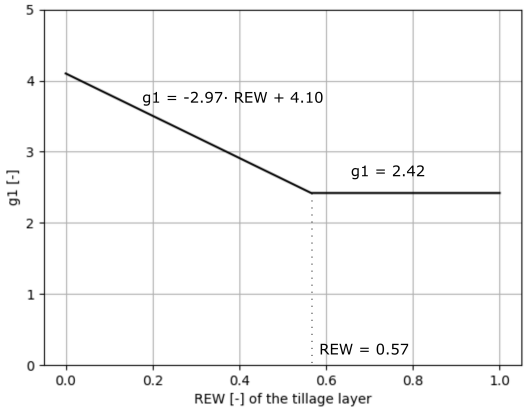

Figure 17: Definition of g_1 as a function of REW

We faced two significant problems while trying to simulate net assimilation for the M0 model. They were both related to the nitrogen dependence of $V_{cmax,25°C}$. The first one was that during the 2018 vegetation season at Lonzée, only one single nitrogen measurement was performed, which is insufficient to define a continuous function all over the growing season. The second problem arises from the calibration of the relation between $V_{cmax,25°C}$ and N. As developed in section 3.1.3, the Bordia experiment did not reveal a significant relation. Because of these two issues, it was decided to perform the simulation on a restricted period when the N leaf content, and then the $V_{cmax,25°C}$, can be considered constant and equal to 90.74 ± 2.29 $\mu molm^{-2}s^{-1}$, $p < 0.01$). This period is comprised between DaE 42 to 62 (see Figure 18) and has been defined during a previous study on the same dataset (Beauclaire, personal communication). It can be noted that this unstressed value obtained is very close to the one defined at Bordia with a different method (98.96 $\mu molm^{-2}s^{-1}$).

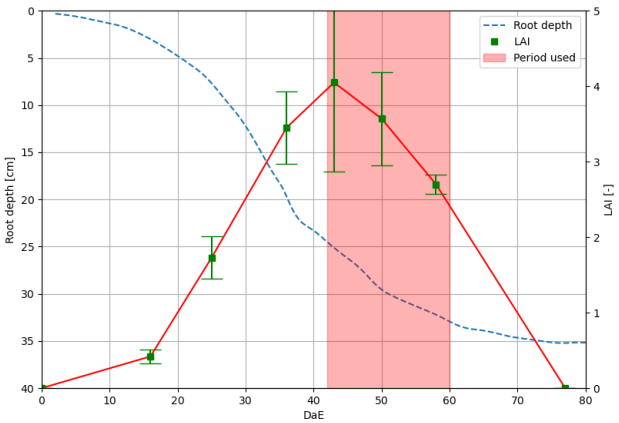

Figure 18: LAI and estimated rooting depth as a function of DaE as well as period used for simulation

The computation of REW required knowledge of the rooting depth. The latter can be obtained using the equations described in Hartmann et al. 2018. The evolution of simulated rooting depth at Lonzée is presented in Figure 18 (Beauclaire personal communication). It can be seen that the root system of potatoes has almost reached its full development (root depth higher than 25 cm) on the restricted period considered. Therefore, it allowed a REW computation based on average SWC measurements from the soil surface to 30 cm depth of soil.

3.2.2 Comparison of performances of the two models for the whole period

Simulation results for M0 and M2 are presented for the entire period in Appendices G and H. The ability of the models to predict the observed assimilations are reported in Figure 19. These observations are derived from EC gap-filled and partitioned measurements to provide the gross primary production (GPP). The RMSE was calculated on a daily basis, and the REW was added to the graph.

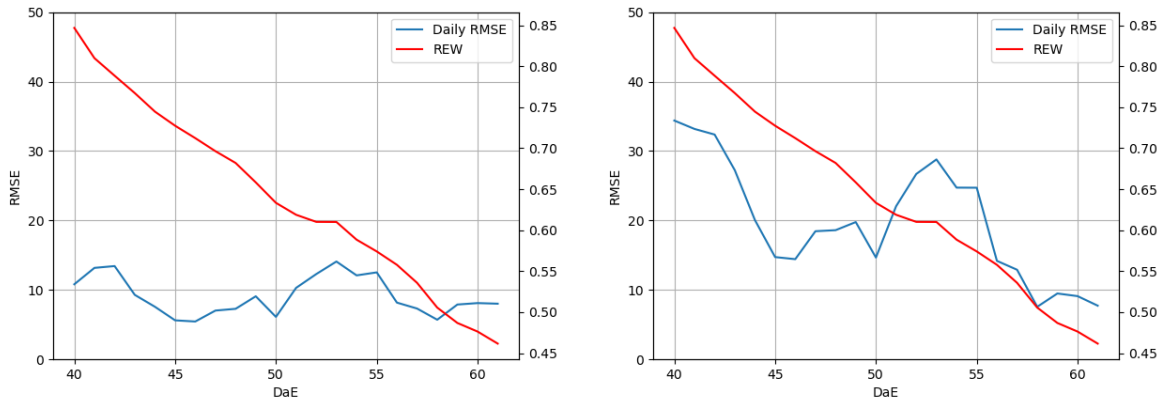

(a) (b)

Figure 19: Evolution of the REW as well as the daily RMSE between the model and the gapfilled flux values for M0 (a) and M2 (b) models

M0 globally performs better than M2. Contrary to what was expected, its error does not seem to increase with decreasing REW. M2 gave less accurate results at the beginning of the modelling period (unstressed situation), and its predictive capabilities seemed to be improved when the REW decreases. However, it did not significantly improve the prediction capabilities when REW was low compared to M0.

It can be noticed that the error increased significantly for M2 at two defined periods (40-45 and 50-55). This phenomenon is also visible for M0 but less markedly. This increase in error is due to an overestimation of simulated assimilation compared to the GPP calculated by REddyProc, as shown in the graph in Appendix G.

3.2.3 Comparison of performances on the intra-day dynamics

The Lonzée 2018 dataset was split into a stressed and an unstressed period following a REW threshold value equal to 0.6, and the predicted and observed daily fluctuations of the assimilation were deduced by averaging values of all the similar half-hours from the different days of the period. The result is available in figure 20.

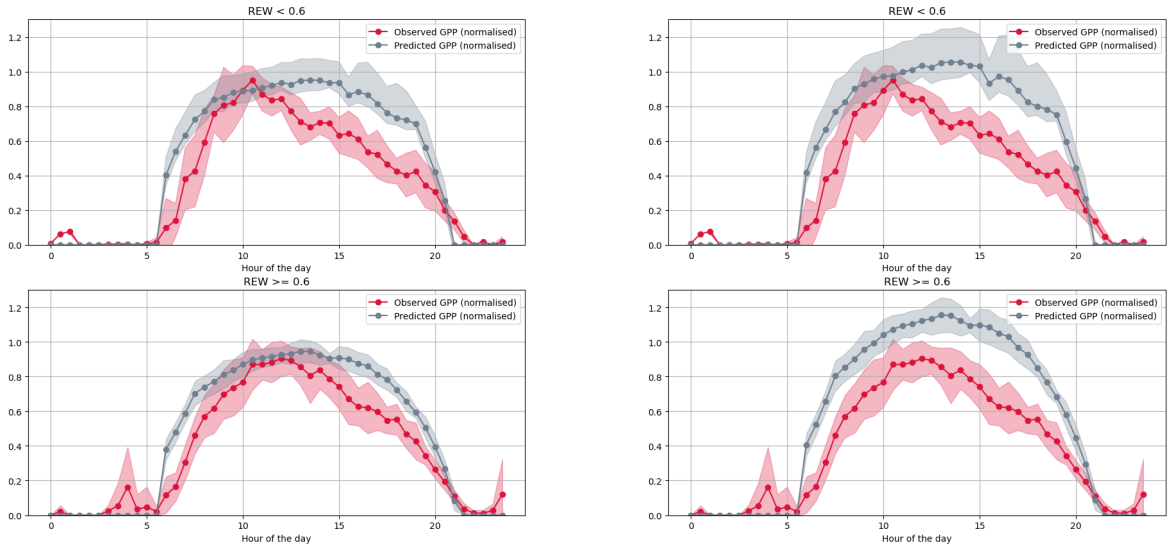

(a) (b)

Figure 20: Averaged intraday dynamics of predicted and observed assimilations for stressed and unstressed plants and for M0 model (a) and M2 model (b)

It can be seen that both versions of the model failed to account for intraday dynamics for both stressed and unstressed periods. As a result, they overestimate the assimilation at the beginning and end of the day. M0 better reproduced the mid-day values with or without edaphic stress. Observed GPP shows two utterly different behaviours in the presence and absence of water stress. When edaphic stress occurs, assimilation increases until it reaches a maximum at about 10 AM. Once this maximum is passed, it decreases linearly until the end of the day. Neither of the two models has been able to reproduce the behaviour.

4 Discussion

4.1 Nitrogen measurements and relation with $V_{cmax,25°C}$

As explained in Section 2.1.3, $V_{cmax,25°C}$ is often determined from a linear relationship to nitrogen leaf content. Figure 14 shows that we were unable to establish this relationship for both $V_{cmax,25°C,app}$ and $V_{cmax,25∘C,real}$ in this work. This absence of relation is more related to some methodological biases than to the independence between the two parameters. The N analyses were not performed on the same leaves as those chosen for gas exchange measurements. Leaves were chosen to be similar in terms of exposure, size and position in the canopy. However, this choice was made based on visual criteria. There is a possibility that variability between leaves in terms of nitrogen concentration is large enough to confound the regression. The second problem lies in the range of nitrogen values evaluated. The leaves analysed yielded values ranging from 110 to 170 to $\mu molm^{-2}_{leaf}$, which is relatively narrow. Studies seek to establish the relationship between photosynthesis and nitrogen content using much wider ranges by sampling different leaf types with different fertilisation levels. For wheat, for example, a range of 10 to 200 $\mu molm^{-2}_{leaf}$ was used to show a clear relation between nitrogen content and $V_{cmax,app}$ (Evans 1983). For potato, a study was carried out to establish a relation between photosynthesis and nitrogen content with a range of 63 to 189 $\mu molm^{-2}_{leaf}$ (Vos and Oyarzun 1987).

Information on the relationship between $V_{cmax,25°C}$ and N can however be deducted from the graph 13 gives us valuable information on the relationship between N and $V_{cmax,25°C}$. As shown in Section 3.1.3, no significant difference was found between the nitrogen content of the leaves for stressed and unstressed plants. Furthermore, it has been demonstrated that a decrease in $V_{cmax,25°C}$ (apparent and real) appears when the soil water content decreases. It can therefore be deduced that the linear relationship between nitrogen content and $V_{cmax,25°C}$ observed by Evans 1983 and Field and Mooney 1986 is only valid in the case where the plants are not water-stressed. At the model level, this indicates that the linear relationship used initially to define $V_{cmax,25°C}$ is insufficient to capture the dynamics of $V_{cmax,25°C}$ in the face of decreasing soil water availability.

Since the decrease in REW coincides with the decrease in N, it is legitimate to verify whether the reduction in $V_{cmax,25°C,app}/V_{cmax,25°C,real}$ is attributed to edaphic stress. If the reduction was linked to N, $V_{cmax,25°C,app}/V_{cmax,25°C,real}$ values from the unstressed plants would then result in plateau noise and $V_{cmax,25°C,app}/V_{cmax,25°C,real}$ values from the stressed plants would show a linear decrease. The result would be a distribution of raw data points similar to what was observed in the experiment. However, if we disregard the points from the unstressed plants, the sigmoid functions remain highly significant ($p < 0.01$ for both $V_{cmax,25°C,app}$ and $Vcmax, 25°C, real$) and $V_{cmax,25°C,real}$ show a much higher coefficient of determination ($R^2 = 0.8614$). Moreover, analyses carried out on trees that do not show this nitrogen reallocation dynamic (Migita et al. 2007) show the same decrease in $V_{cmax,25°C}$ with soil water content (Gourlez de la Motte et al. 2020).

4.2 C_i measurements and cuticular resistance

For C_i calculation, it is assumed that CO_2 and water vapour diffusion occurs through the stomata. In order to determine g_s for CO_2, g_s for water vapour is determined from the Penman-Monteith equation and then divided by a factor of 1.6. It has been shown that this assumption is not always

valid, especially when plants experience water stress. During these periods, the stomata are entirely closed to avoid too severe water losses. The preferential path for water vapour diffusion is no longer the stomata but the cuticle (Hansen et al. 2010). The cuticular conductance being much higher for water than for CO_2 (Boyer 2015) leads to an overestimation of the CO_2 conductance and thus C_i. This rise up of C_i value lead to an overestimation of $V_{cmax,app}$. Contrastingly, g_m is diminished, which leads to lower values of C_c. The $V_{cmax,real}$, which depends on these two parameters, should be slightly underestimated.

4.3 Evaluation of the dependence between REW and biochemical parameters

4.3.1 Sigmoids interpretation

The shape of the sigmoid seems to represent well the behavior of $V_{cmax,25°C,app}$, $V_{cmax,25°C,real}$ and g_m with respect to REW. These dependencies have also allowed to highlight REW_{stress} values that were not significantly different and to define a threshold at which the edaphic stress becomes impacting for the biochemical parameters equal to 0.6. This threshold is consistent with what has already been determined in the literature. Indeed, it has been shown that when the REW fell below 0.6, the growth of potato leaves was stopped Weisz et al. 1994. This threshold is significantly higher than the 0.4 regularly used for forest ecosystems. It is mainly due to the sensitivity of potato shallow roots to edaphic stress Dahal et al. 2019.

For both $V_{cmax,25°C,app}$ and $V_{cmax,25°C,real}$, the variability observed across the plateau could be related to a dependence on leaf nitrogen content. If this relationship is linear once a certain REW threshold is reached, this could explain the funnel shape of the raw data points at the plateau.

It was noted earlier that $V_{cmax,real}$ value was twice as high as $V_{cmax,app}$ value. It is explained by the difference in concentration between C_i and C_c. Indeed, if we take into account g_m, CO_2 must pass through an additional resistance to reach the Calvin cycle. When the Farquhar et al. 1980 model is used with $V_{cmax,25°C,app}$, it implies the usage of C_i (higher than C_c) and needs then a V_{cmax} value lower to compensate and simulate the same assimilation value.

For g_m, we also see a divergence of the points from the plateau values around REW = 0.9. However, it is much more asymmetric than for $V_{cmax,25°C,apparent}$ or $V_{cmax,25°C,real}$. It seems that the value of the parameter increases again after a certain REW threshold. Several hypotheses have been put forward to explain the phenomenon, but none has proved satisfactory. It was considered that this increase is linked to an increase in leaf temperature, a variation in nitrogen content, an increase in VPD, or an increase in C_a. The dependence with leaf temperature was already considered in Section 2.2.7 and proved to be insignificant. To assess the potential relationship with nitrogen content, a linear regression was applied. The fit was found to be non-significant, but doubt remains due to the methodological biases mentioned above. This increase cannot be explained by C_a as its value was essentially identical for each measurement. Since the VPD depends on RH that was not fixed during the acquisition, it is plausible that this factor influences the increase of the parameter. Another hypothesis that can be put forward is that this increase is part of g_m behaviour, non explained with the sigmoid function.

4.3.2 Sigmoids uncertainties

The construction of the sigmoids as described above is very sensitive to the choice of classes limits and outliers removal methods. The choice of the breakpoint in the range of its uncertainty has little influence on the regression because there is no data with REW values in this range (no value between 0.55 and 0.65). Determining the REW classes limits provides the same results for any breakpoint chosen between these two values.

In contrast, the number of classes on each side of this breakpoint significantly influences the regression quality. For example, by taking more classes, each class has fewer points and therefore, the standard deviation decreases. If the standard deviation for a class becomes very close to 0, it gives it a very high weight and forces the regression to pass through this point.

For the filter method, it turns out that the factor by which the multiplier on the MAD is multiplied to fix the limit for outliers can have a significant impact on the standard deviation of mean values for each class and, therefore, the weight in the regression. The application of a factor of 2 leads to an average removal of 11% of the data. The most impacted parameter is $\mathrm{g_m}$ with a 15% reduction of the dataset. Even though the LICOR6400-XT sources of error are numerous and can lead to considerable variability in the results, a more conservative threshold of 3 times the MAD has been retained. This threshold leads to the removal of 3.5% of the data (8% for $\mathrm{g_m}$). When applying a more restrictive threshold, especially for $\mathrm{g_m}$ parameter and stressed plants, induce a very low standard deviation which sometimes leads to an impossibility for the regression algorithm to converge.

As shown above, the curvature factor is always non-significant. It exists other relations with globally the same behavior that may not require this parameter. For example bilinear relations have already been used to show the dependence between $\mathrm{V_{cmax,25°C}}$ and soil water content (Gourlez de la Motte et al. 2020). It is composed of a linear growth phase followed by a plateau and requires adjusting four parameters (plateau value, breakpoint, slope and intercept for the growth phase).

4.4 Leaf scale modelling

The systematic underestimation of assimilation by M1 scenario is explained by the low value of $\mathrm{V_{cmax,25°C,app}}$. As part of the optimisation attempt, we sought to find a constant value of $\mathrm{V_{cmax,25°C,app}}$ that would minimise the error on all the curves. The value obtained was 125 $\mu\mathrm{molm^{-2}s^{-1}}$ which is well above the sigmoid plateau defined for $\mathrm{V_{cmax,25°C,app}}$ (98.96 $\mu\mathrm{molm^{-2}s^{-1}}$). If the value at the plateau is too low, it could limit the assimilations.

As it has been seen in Section 3.1.4, the scatterplot of M2 predictions showed a bilinear behaviour with important overestimation at low assimilation values. As this overestimation occurs in the assimilation range for which $\mathrm{J_{max}}$ is limiting, two elements can explain this observation. The first one is the absence of a potato calibrated value of curvature parameter ϑ_1. For all the simulations, it was set at the value defined for wheat. An overestimation of this parameter could lead to a surestimation of $\mathrm{J_{max}}$. The second hypothesis is related to the potential dependence of $\mathrm{g_m}$ on $\mathrm{C_i}$. During the experiment, for the determination of $\mathrm{g_m}$ (one-shot data), the measurements were acquired with a constant $\mathrm{C_a}$ value equal to 400 ppm. Flexas et al. 2007 conclude that $\mathrm{g_m}$ is $\mathrm{C_a}$ and PPFD dependent. PPFD was kept at 1500 $\mu\mathrm{molm^{-2}s^{-1}}$ for both $\mathrm{A_n}$-$\mathrm{C_i}$ curves and one-shot dataset. When there were some

variations of C_i in A_n-C_i curves, g_m seems to have decreased when low C_i values have been applied which led to reduction of the assimilation not taken into account in the model with a g_m independent of C_a. The only source of variation that could explain the phenomenon comes from the variation of C_i in A_n-Ci curves. In our case, g_m seems to be underestimated for low C_i values which lead to an underestimation of the observed A_n values. According to Flexas et al. 2007, for some plants in C3, g_m is positively correlated with PPFD and negatively with C_i.

The predicted assimilation is much lower for low REW values (less than 0.3) than for the observed one. However, this is much less marked than for the first model.

4.5 Ecosystem scale modelling

4.5.1 Overall dynamic

There are strong indications that the poor reproduction of the influence of diffuse radiation is responsible for the two peaks in RMSE corresponding to an overestimation of CO_2 assimilation observed during the M2 simulation at ecosystem scale (see Figure 19, DaE 40-45 and 50-55). The temporal evolution of the daily RMSE for M2 simulation and the graph of the evolution of diffuse radiation are reported in figure 21. There is an obvious correspondence between high RMSE (overestimation) and high diffuse PPFD. Diffuse PPFD plays a role in limiting the net assimilation when this last is limited by electron transport (J_{max}). Therefore, two hypotheses can be put forward to explain this phenomenon. The first one is an overestimation of the diffuse radiation absorbed by the leaves. However, this seems unlikely since the only change that can drastically decrease the diffuse PPFD absorption is an increase of the clumping factor C, but it is equal to 1, which is its maximum value.

The second hypothesis is based on a potential overestimation of the J_{max} variable in the one-shot dataset which lead to a too high multiplicative coefficient when computing $J_{max,25°C}$ from $V_{cmax,25°C,real}$. A value of J_{max} that is too high and consequently a rise in the assimilation when limited by J_{max} could explain this phenomenon. When diffuse radiation is high, this overestimation can even lead to a passage, in the model, from an electron transport limitation to a Rubisco activity one (if A_j passes over A_v). The difference in performance over these periods between the two models (M0 giving better results than M2) may be related to the better calibration of the multiplicative factor used to define J_{max} from V_{cmax} in the $V_{cmax,25°C,app}$ case comparing the $V_{cmax,25°C,real}$ one. It corroborates the observations already made at the leaf level.

The graph also highlights that below a certain REW threshold, the error no longer seems to be related to diffuse PPFD. It can be explained by the fact that other factors are limiting photosynthesis during this period (REW and VPD for M2, VPD for M0), which prevents the assimilations from increasing too much by limiting V_{cmax} and indirectly J_{max} when edaphic stress occurs.

It has been suggested that Chloroplasts can have very different light conditions depending on their distance from the leaf surface (Buckley and Farquhar 2004). Furthermore, recent development in the field of 3D mesophyll modelling showed that not taking into account this dispersion of chloroplasts within the mesophyll can lead to errors in the estimation of J, mainly when diffuse radiation is high Xiao et al. 2016. Attempts to overcome this problem have been proposed by defining a transdermal absorption profile (Buckley and Farquhar 2004). Taking these considerations into account in a future

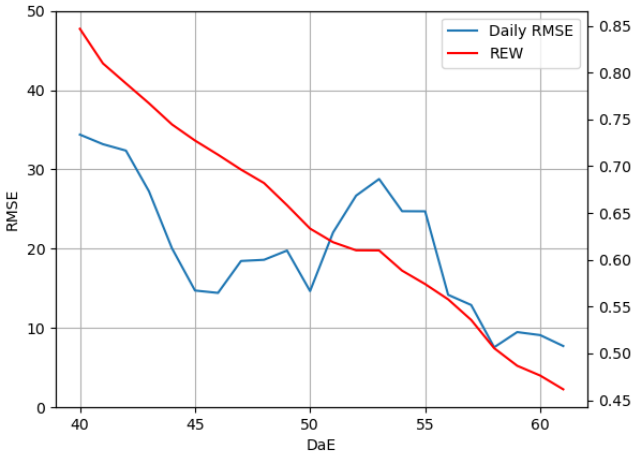

(a)

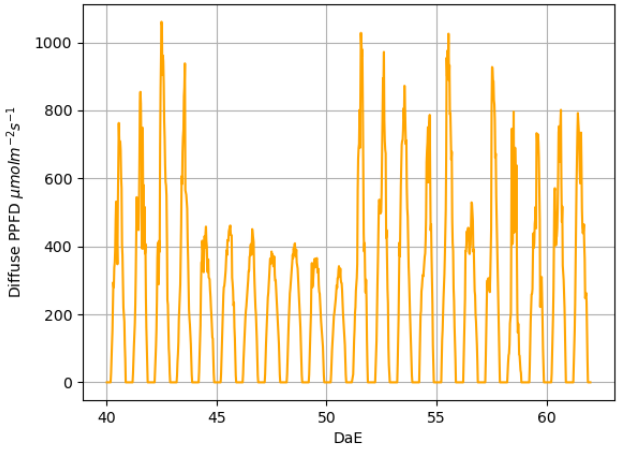

(b)

Figure 21: RMSE related to the model with $V_{cmax,25°C,real}$ and g_m depending on REW and diffuse PPFD observed for the whole period of simulation

model could reduce the experimental error when diffuse radiation increases and better monitor intra-day dynamics.

4.5.2 Intra-days dynamic

It has been shown that M0 and M2 systematically overestimated assimilation at the end and beginning of the day (see Figure 20). Solar radiation during these periods is relatively low, and chloroplasts do not reach a state of light saturation. In the model, this results in a limitation of assimilation by J_{max}. This overestimation related to J_{max} seems to be in line with what has already been discussed for the overall dynamic simulation.

The overestimation at mid-day assimilation for M2 scenario is explained by the potentially too

high value of $V_{cmax,real}$ defined with Bordia data. As V_{cmax} is the limiting factor in the middle of the day when the irradiance saturates the photosynthetic apparatus, its overestimation leads to a higher limiting threshold on assimilation and an increase in the latter. It is also possible that this overestimation of assimilation is linked to a poor estimation of the g_m parameter as reported before due to its potential dependence on C_a. An overestimation of g_m could lead to an overestimation of C_c. As C_c is directly linked to V_{cmax}, an increase in the latter leads to an overestimation of assimilation.

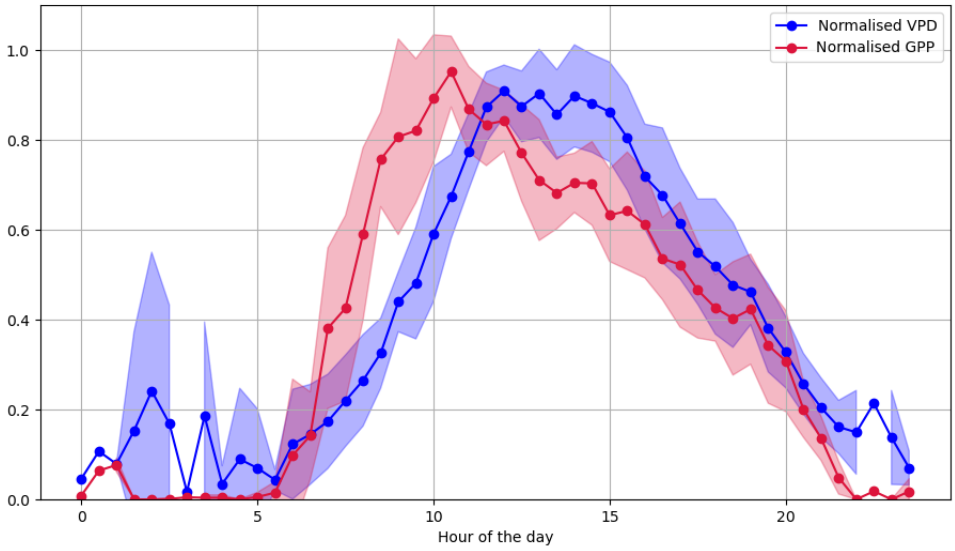

Figure 22: Normalised GPP of stressed plants observed at Lonzée and normalised VPD for the same period

Figure 22 demonstrated that the asymmetric triangular shape showed by the observed assimilation during edaphic stress seems to be related to the VPD. When edaphic stress occurs, the amount of water available in the atmosphere often also becomes scarcer. Figure 22 shows the mean daily variation of normalised GPP and VPD values with respect to their daily maximum value for the period of the simulation when the REW is below 0.6 (threshold defined from analysis performed at section 3.1.1). It can be seen that the significant decrease in GPP after 10 AM, whereas PPFD is still increasing, coincides with the higher values for VPD. As the demand for water from the atmosphere increases, the plant closes its stomata to minimise water losses, which results in a slowing down of CO_2 diffusion and a decrease in assimilation. It seems that the model poorly represents this dependence between atmospheric water demand and stomatal closure during edaphic stress. This dependence is represented by the slope parameter g_1 (that seems too large) in the Medlyn et al. 2011 stomatal model (cfr. equation 5). The dependence of g_1 on REW seems to lead to a g_1 overestimation for low REW, which prevent g_s from decreasing sufficiently when VPD increases during low REW periods.

4.5.3 Model uncertainties

Some model parameters (Γ, $\Gamma^*_{25°C}$, ϑ_j) could not be determined for potato from the data acquired during the Bordia experiment. The calibration of Farquhar et al. 1980 model could only be done incompletely. An attempt was made to calibrate the A_n-Ci curves by optimising several parameters at the same time with the Broyden-Fletcher-Goldfarb-Shanno algorithm. However, the lack of convergence led to a sensitivity analysis before optimising each parameter from the most sensitive to the least sensitive. This last attempt also proved unsuccessful. The approach and the results obtained are available in Appendix F. It was finally decided to keep the parameterisation performed by De Pury and Farquhar 1997 for wheat.

By using a simple ratio to define $J_{max,25°C}$, we assume that the dynamics regarding REW is the same for $V_{cmax,25°C,real}$ or $V_{cmax,25°C,app}$ and $J_{max,25°C}$. We have been able to show two relatively different dynamics for $V_{cmax,25°C,app}$ and $V_{cmax,25°C,real}$ at Section 3.1.1. It would perhaps be more judicious during future development to determine an independent relation for $J_{max,25°C}$.

4.5.4 Validation data uncertainties

The GPP used for the model validation was obtained by the partitioning method described in Section 2.5 with the REddyProc R package. This partitioning is performed by using a relation between R_{eco} and air temperature. When an edaphic stress occurs, R_{eco} decreases. Thus, for a same temperature, the predicted R_{eco} is larger than the actual one. GPP being determined by the net flux and the predicted R_{eco}, an overestimation of R_{eco} leads to an overestimation of GPP.

4.6 Uncertainties related to $V_{cmax,app}$, $V_{cmax,real}$, J_{max} and g_m determinations

4.6.1 Impact of R_d estimation on $V_{cmax,app}$ and $V_{cmax,real}$

As described above, R_d is involved in the calculation of $V_{cmax,app}$ and $V_{cmax,real}$. As it was not acquired during the experiment, finding a way to estimate it was necessary. It is usual to neglect this term when trying to determine $V_{cmax,app}$ from assimilation values at light saturation. Indeed, in this case, the carbon flux linked to photosynthetic activity is prominent compared to mitochondrial respiration. Other estimation methods such as the one presented above and used in this work are based on a linear relation in R_d and $V_{cmax,app}$ (De Kauwe et al. 2016). Another possibility that was also considered in this work was to replace R_d by its fundamental expression deduced from equation 15 and Arrhenius expression (equation 9) in the equations 38 and 39 and finally isolate V_{cmax} in the obtained expression. It can be translated into the following equation for $V_{cmax,app}$:

$$V_{cmax,app} = \frac{A_n(K' + C_i)}{(C_i - \Gamma^*)(1 - \frac{\Gamma - \Gamma^*}{\Gamma + K'} \cdot e^{1600 \cdot \frac{T - 298.15}{298.15RT}} \cdot \frac{C_i + K'}{C_i - \Gamma^*})} \tag{46}$$

And for $V_{cmax,real}$:

$$V_{cmax,real} = \frac{A_n(K' + C_c)}{(C_c - \Gamma^*)(1 - \frac{\Gamma - \Gamma^*}{\Gamma + K'} \cdot e^{1600 \cdot \frac{T - 298.15}{298.15RT}} \cdot \frac{C_c + K'}{C_c - \Gamma^*})} \tag{47}$$

The usage of this method for $V_{cmax,app}$, led to values 4% lower compared to values returned by De Kauwe et al. 2016 method. For $V_{cmax,real}$, these discrepancies raised up to 14 %. Therefore, it seems that these estimation methods that have been developed for $V_{cmax,app}$ are relevant.

There is a fourth possibility to determine R_d. Indeed, it is possible to extract its value by fitting Farquhar et al. 1980 equations on A_n-C_i curves. This method is considered more precise than simply computing R_d by considering a fraction of $V_{cmax,app}$ (De Kauwe et al. 2016). It has been considered to use A_n-C_i curves with the Plantecophys package available in R (Duursma 2015). However, this method would induce a bias in model validation due to the A_n-C_i curves dataset used for validation and calibration. Nevertheless, estimations of both $V_{cmax,app}$ and $V_{cmax,real}$ with this method show higher values on average (respectively 29% and 18% higher). It suggests that the method used to determine R_d in this study tends to underestimate $V_{cmax,app}$ and $V_{cmax,real}$.

It would have been interesting to perform R_d measurements with the LICOR6400-XT in parallel with acquiring the one-shot data and the A_n-C_i curves for completeness. However, these measurements can be performed by setting the PPFD to 0 in the measurement cell and acquiring the CO_2 flux values after an adaptation time.

4.6.2 Impact of K_c, K_o and Γ^* on $V_{cmax,real}$

To determine $V_{cmax,real}$, activation energy and value at 25°C for K_c, K_o and Γ^* were determined based on Bernacchi et al. 2001. These values were determined using the gas exchange method and by considering g_m as infinite, so that only $V_{cmax,app}$ was calibrated. Although these values are mostly considered valid for $V_{cmax,real}$, they may lead to some inaccuracies in the modelling. According to Knauer et al. 2020, the use of these values may lead to a higher sensitivity of V_{cmax} to C_i when g_m is taken into account. It may result in an overestimation of $V_{cmax,real}$ compared to its true value. Nevertheless, it would be wise to re-evaluate these parameters from chloroplast suspensions instead of gas-exchange measurements (Badger and Collatz 1977) with modern analytical chemistry methods.

4.6.3 Fluorescence measurements uncertainties

In this work, we determined J_{max} using fluorescence measurements made with the LICOR6400-40 fluorometer. This measurement of J_{max} allowed to calculate g_m and C_c. Fluorescence measurements also have an impact on $V_{cmaxreal}$ calculation given that C_c is involved in its determination. The method is based on the assumption that the ratio between photosynthetic capacity and absorbed radiation ($\alpha\beta$) is constant within the leaf. It is equivalent to considering that the $\alpha\beta$ product is the same for all chloroplasts.

It is known that chloroplasts are non-uniformly distributed within the mesophyll. The position of chloroplasts at different depths within the mesophyll subjects them to different light conditions, resulting in different characteristics (Chlorophyll a/b ratio, Rubisco content) (Terashima and Inoue 1985). At room temperature, chlorophyll can fluoresce between 686 and 740 nm (Evans 2009). Chlorophyll does not have the same absorbance for these different wavelengths. It is 0.92 at 680 nm and decreases almost linearly to 0.14 at 735 nm (Xiao et al. 2016). The fluorometer used has a filter that allows capturing the radiation emitted at 715 nm. By performing linear interpolation on this data, the absorbance of chlorophyll can be estimated to be 0.44. This result suggests that the fluorescence signal obtained

is a mixture of emission and absorption of chloroplasts located at different depths and with different characteristics. The assumption that is made may therefore lead to incorrect values of $\mathrm{J_{max}}$, $\mathrm{g_m}$, $\mathrm{C_c}$ and $\mathrm{V_{cmax,real}}$. This can explained the greater variability of $\mathrm{V_{cmax,real}}$ data compared to $\mathrm{V_{cmax,app}}$ ones.

Evans 2009, also suggests that the dependence that has been observed between irradiance and $\mathrm{g_m}$ as well as $\mathrm{C_i}$ and $\mathrm{g_m}$ is related to these uncertainties in the fluorescence measurements.

5 Conclusion

This study aimed to determine whether the implementation of new assumptions within the Farquhar et al., 1980 model would improve prediction capabilities during drought events. These assumptions were the inclusion of a mesophyll resistance (g_m) which is still absent in most terrestrial ecosystem models, and dependence between the maximum carboxylation rate (V_{cmax}) and the soil water content.

V_{cmax} is the main parameter of terrestrial ecosystem assimilation models. Initially, it depended only on leaf nitrogen content. The experiment carried out at Bordia confirmed the decrease in the parameter with the onset of water stress, whether g_m is taken into account or not.

A sigmoid fit was performed between these parameters and the soil water availability. This availability was defined with a normalised soil water content or relative extractable water (REW). These adjustments were found to be highly significant for $V_{cmax,real}$, $V_{cmax,apparent}$ and g_m. For the first two, we notice a significant variability at the plateau, which could be attributed to the nitrogen content of the leaf. However, this last point could not be verified clearly and definitively. Furthermore, for g_m, it seems that part of the dynamics when REW was not limiting is not well captured by the sigmoid.

These sigmoids allowed the determination of a REW threshold above which potato plant is not affected by water stress. The monitoring of biochemical parameters carried out during this study suggests that this threshold is comprised between 0.53 and 0.6 for potato.

These sigmoids were implemented in the Farquhar et al., 1980 model at the leaf scale. The results show better performance when using g_m in the conductance scheme as well as a $V_{cmax,real}$, both depending on the REW. However, it was pointed out that some uncertainty in the determination of g_m and J_{max} tends to decrease the gain for low CO_2 values. A slight offset error was also observed, which suggests that the V_{cmax} acquisition method overestimates its actual value. The simulation with $V_{cmax,app}$ gave much worse results suggesting that its use should be abandoned to estimate assimilation during water stress.

A second simulation was carried out at the ecosystem scale. For this simulation, the initial model with the model taking into account g_m and $V_{cmax,real}$ have been compared. The latter proved to be less efficient on average and did not increase the quality of predictions even at low REW content. The model overestimates the assimilations on average, probably due to an overestimation of V_{cmax} in the Bordia experiment.

This second simulation also allowed us to highlight other sources of error exogenous to the present work. The analysis of the intra-day dynamics thus highlighted an excessively high value of g_1 and a potential overestimation of J_{max}.

There are still many areas for improvement in the model. It would be interesting to introduce a complete model of light absorption, which would take into account the dispersion of chloroplasts within the mesophyll and an expression of J_{max} independent of V_{cmax}.

References

Badger, M.R. and G.J. Collatz, (1977). Studies on the kinetic mechanisme of Ribulose-1,5-Biphosphate Carboxylase and Oxygenace reactiions, with particular reference to the effect of temperature on kinetic parameters. In: *Carnegie Institute of Washington Yearbook* **76**, pp. 355–361.

Ball, J.T., I.E. Woodrow, and J.A. Berry, (1987). A Model Predicting Stomatal Conductance and its Contribution to the Control of Photosynthesis under Different Environmental Conditions. In: *Progress in Photosynthesis Research*. Ed. by J. Biggins. Dordrecht: Springer Netherlands, pp. 221–224.

Bernacchi, C.J. et al., (2001). Improved temperature response functions for models of Rubisco-limited photosynthesis. In: *Plant, Cell & Environment* **24**, pp. 253–259.

Bernier, P.Y. et al., (2006). Drought constraints on transpiration and canopy conductance in mature aspen and jack pine stands. In: *Agricultural and Forest Meteorology* **140**, pp. 64–78.

Black, T.A., (1979). Evapotranspiration from Douglas fir stands exposed to soil water deficits. In: *Water Resources Research* **15**.1, pp. 164–170.

Bonan, G.B. et al., (2014). Modeling stomatal conductance in the earth system: linking leaf water-use efficiency and water transport along the soil–plant–atmosphere continuum. In: *Geoscientific Model Development* **7**.5, pp. 2193–2222.

Boyer, J.S., (2015). Turgor and the transport of CO2 and water across the cuticle (epidermis) of leaves. In: *Journal of Experimental Botany* **66**.9, pp. 2625–2633.

Breda, N., A. Granier, and G. Aussenac, (1995). Effects of thinning on soil and tree water relations, transpiration and growth in an oak forest (Quercus petraea (Matt.) Liebl.) In: *Tree Physiology* **15**.5, pp. 295–306.

Buckley, T.N. and G.D. Farquhar, (2004). A new analytical model for whole-leaf potential electron transport rate. In: *Plant, Cell and Environment* **27**.12, pp. 1487–1502.

Cadule, P. et al., (2010). Benchmarking coupled climate-carbon models against long-term atmospheric CO $_2$ measurements. In: *Global Biogeochemical Cycles* **24**.2, pp. 1–24.

Calvet, J.-C. et al., (2004). Modelling forest transpiration and CO2 fluxes—response to soil moisture stress. In: *Agricultural and Forest Meteorology* **124**.3, pp. 143–156.

Canadell, J.G. et al., (2007). Contributions to accelerating atmospheric CO2 growth from economic activity, carbon intensity, and efficiency of natural sinks. In: *Proceedings of the National Academy of Sciences* **104**.47, pp. 18866–18870.

Christidis, N. and P.A. Stott, (2014). Change in the Odds of Warm Years and Seasons Due to Anthropogenic Influence on the Climate. In: *Journal of Climate* **27**, p. 15.

Coumou, D. and A. Robinson, (2013). Historic and future increase in the global land area affected by monthly heat extremes. In: *Environmental Research Letters* **8**.3, pp. 1–7.

Cowan, I.R. and G.D. Farquhar, (1977). Stomatal function in relation to leaf metabolism and environment. In: *Integration of Activity in the Higher Plant*. Ed. by Jennings DH. Cambridge: Cambridge University Press, pp. 471–505.

Cowan, I.R. and F.L. Milthorpe, (1968). Plant Factors Influencing the Water Status of Plant Tissues. In: *Water Deficits and Plant Growth*. T. T. Kozlowski. Vol. 1. Academic Press, Inc.

Dahal, K. et al., (2019). Improving Potato Stress Tolerance and Tuber Yield Under a Climate Change Scenario – A Current Overview. In: *Frontiers in Plant Science* **10**, pp. 1–16.

De Kauwe, M.G. et al., (2015). A test of an optimal stomatal conductance scheme within the CABLE land surface model. In: *Geoscientific Model Development* **8**.2, pp. 431–452.

De Kauwe, M.G. et al., (2016). A test of the 'one-point method' for estimating maximum carboxylation capacity from field-measured, light-saturated photosynthesis. In: *New Phytologist* **210**.3, pp. 1130–1144.

De Pury, D.G.G. and G.D. Farquhar, (1997). Simple scaling of photosynthesis from leaves to canopies without the errors of big-leaf models. In: *Plant, Cell and Environment* **20**.5, pp. 537–557.

Deblonde, P.M.K. and J.F. Ledent, (2001). Effects of moderate drought conditions on green leaf number, stem height, leaf length and tuber yield of potato cultivars. In: *European Journal of Agronomy* **14**, pp. 31–41.

Delhez, L., (2019). *Mechanistic modelling of cropland and grassland ecosystems: focus on the carbon cycle and on plant phenology*, p. 106.

Dewar, R.C., (2002). The Ball-Berry-Leuning and Tardieu-Davies stomatal models: synthesis and extension within a spatially aggregated picture of guard cell function: BBL × TD stomatal conductance model. In: *Plant, Cell & Environment* **25**.11, pp. 1383–1398.

Ding, R. et al., (2013). Evapotranspiration measurement and estimation using modified Priestley–Taylor model in an irrigated maize field with mulching. In: *Agricultural and Forest Meteorology* **168**, pp. 140–148.

Dore, M.H.I., (2005). Climate change and changes in global precipitation patterns: What do we know? In: *Environment International* **31**.8, pp. 1167–1181.

Drake, B.G., M.A. Gonzàlez-Meler, and S.P. Long, (1997). More Efficient Plants : A Consequence of Rising Atmospheric CO $_2$? In: *Annual Review of Plant Physiology and Plant Molecular Biology* **48**.1, pp. 609–639.

Drake, J.E. et al., (2017). Stomatal and non-stomatal limitations of photosynthesis for four tree species under drought: A comparison of model formulations. In: *Agricultural and Forest Meteorology* **247**, pp. 454–466.

Duursma, R.A., (2015). Plantecophys - An R Package for Analysing and Modelling Leaf Gas Exchange Data. In: *Plos One* **10**.11. Ed. by Paul C. Struik, pp. 1–13.

Evans, J.R., (1983). Nitrogen and Photosynthesis in the Flag Leaf of Wheat (*Triticum aestivum* L.) In: *Plant Physiology* **72**.2, pp. 297–302.

Evans, J.R., (2009). Potential Errors in Electron Transport Rates Calculated from Chlorophyll Fluorescence as Revealed by a Multilayer Leaf Model. In: *Plant and Cell Physiology* **50**.4, pp. 698–706.

FAOSTAT, (2021). *World production of potato in 2019*. URL: %5Curl%7Bhttp://www.fao.org/faostat/fr/#data/QC%7D. Accessed on 7th June 2021.

Farquhar, G. D., S. von Caemmerer, and J. A. Berry, (1980). A biochemical model of photosynthetic CO2 assimilation in leaves of C3 species. In: *Planta* **149**.1, pp. 78–90.

Field, C.B. and H.A. Mooney, (1986). Photosynthesis–nitrogen relationship in wild plants. In: *On the Economy of Plant Form and Funetion*, pp. 25–55.

Flexas, J. et al., (2007). Rapid variations of mesophyll conductance in response to changes in CO $_2$ concentration around leaves. In: *Plant, Cell & Environment* **30**.10, pp. 1284–1298.

Flexas, J. et al., (2012). Mesophyll diffusion conductance to CO2: An unappreciated central player in photosynthesis. In: *Plant Science* **193**, pp. 70–84.

Friend, A.D. and N.Y. Kiang, (2005). Land Surface Model Development for the GISS GCM: Effects of Improved Canopy Physiology on Simulated Climate. In: *Journal of Climate* **18**.15, pp. 2883–2902.

Galmés, J., H. Medrano, and J. Flexas, (2007). Photosynthetic limitations in response to water stress and recovery in Mediterranean plants with different growth forms. In: *New Phytologist* **175**.1, pp. 81–93.

Geider, R.J. et al., (2001). Primary productivity of planet earth: biological determinants and physical constraints in terrestrial and aquatic habitats: NPP and CLIMATE CHANGE. In: *Global Change Biology* **7**.8, pp. 849–882.

Genty, B., J.-M. Briantais, and N.R. Baker, (1989). The relationship between the quantum yield of photosynthetic electron transport and quenching of chlorophyll fluorescence. In: *Biochimica et Biophysica Acta (BBA) - General Subjects* **990**.1, pp. 87–92.

Gourlez de la Motte, L. et al., (2020). Non-stomatal processes reduce gross primary productivity in temperate forest ecosystems during severe edaphic drought. In: *Philosophical Transactions of the Royal Society B: Biological Sciences* **375**, pp. 1–11.

Granier, A., P. Biron, and D. Lemoine, (2000). Water balance, transpiration and canopy conductance in two beech stands. In: *Agricultural and Forest Meteorology* **100**, pp. 291–308.

Granier, A. et al., (1999). A lumped water balance model to evaluate duration and intensity of drought constraints in forest stands. In: *Ecological Modelling* **116**, pp. 269–283.

Granier, A. et al., (2007). Evidence for soil water control on carbon and water dynamics in European forests during the extremely dry year: 2003. In: *Agricultural and Forest Meteorology* **143**, pp. 123–145.

Grigorieva, Ea, A Matzarakis, and Cr de Freitas, (2010). Analysis of growing degree-days as a climate impact indicator in a region with extreme annual air temperature amplitude. In: *Climate Research* **42**.2, pp. 143–154.

Gudmundsson, L. and S.I. Seneviratne, (2016). Anthropogenic climate change affects meteorological drought risk in Europe. In: *Environmental Research Letters* **11**.4, pp. 1–9.

Hansen, J. et al., (2010). Globale surface temperature change. In: *Reviews of Geophysics* **48**, pp. 1–29.

Hari, P. et al., (1986). Optimal control of gas exchange. In: *Tree physiology* **2**, pp. 169–175.

Hartmann, A. et al., (2018). Implementation and Application of a Root Growth Module in HYDRUS. In: *Vadose Zone Journal* **17**.1, pp. 1–16.

Héroult, A. et al., (2013). Optimal stomatal conductance in relation to photosynthesis in climatically contrasting *Eucalyptus* species under drought: Stomatal responses of eucalyptus under drought. In: *Plant, Cell & Environment* **36**.2, pp. 262–274.

Hirose, T. and M.J.A. Werger, (1987). Nitrogen use efficiency in instantaneous and daily photosynthesis of leaves in the canopy of a Solidago altissima stand. In: *Physiologia Plantarum* **70**.2, pp. 215–222.

Hsiao, T.C., (1973). Plant Responses to Water Stress. In: *Annual Review of Plant Physiology* **24**, pp. 519–570.

IPCC, (2007). Summary for Policymakers. In: *Climate Change 2007: The Physical Science Basis. Contribution of Working Group I to the Fourth Assessment Report of the Intergovernmental Panel on Climate Change*. Ed. by S. Solomon et al. Cambridge, United Kingdom and New York, NY, USA: Cambridge University Press. Chap. SPM.

IPCC, (2013). Summary for Policymakers. In: *Climate Change 2013: The Physical Science Basis. Contribution of Working Group I to the Fifth Assessment Report of the Intergovernmental Panel on Climate Change*. Ed. by T.F. Stocker et al. Cambridge, United Kingdom and New York, NY, USA: Cambridge University Press. Chap. SPM.

IPCC, (2014). Summary for Policymakers. In: *Climate Change 2014: Synthesis Report. Contribution of Working Groups I, II and III to the Fifth Assessment Report of the Intergovernmental Panel on Climate Change*. Ed. by R.K. Pachauri and L.A. Meyer. Geneva, Switzerland.

Johnson, F., H. Eyring, and R. Williams, (1942). The nature of enzyme inhibitions in bacterial luminescence: sulphanilamide, urethane, temperature, pressure. In: *Journal of Cell Comparative Physiology* **20**, pp. 247–268.

Jones, H.G., (1998). Stomatal control of photosynthesis and transpiration. In: *Journal of Experimental Botany* **49**, pp. 387–398.

Kaiser, W.M., (1987). Effects of water deficit on photosynthetic capacity. In: *Physiologia Plantarum* **71**.1, pp. 142–149.

Katul, G.G., S. Palmroth, and R. Oren, (2009). Leaf stomatal responses to vapour pressure deficit under current and CO $_2$ -enriched atmosphere explained by the economics of gas exchange. In: *Plant, Cell & Environment* **32**.8, pp. 968–979.

Keenan, Trevor, Santi Sabate, and Carlos Gracia, (2010). Soil water stress and coupled photosynthesis–conductance models: Bridging the gap between conflicting reports on the relative roles of stomatal, mesophyll conductance and biochemical limitations to photosynthesis. In: *Agricultural and Forest Meteorology* **150**.3, pp. 443–453.

Kirschbaum, M.U.F., (1999). CenW, a forest growth model with linked carbon, energy, nutrient and water cycles. In: *Ecological Modelling* **118**.1, pp. 17–59.

Knauer, J. et al., (2020). Mesophyll conductance in land surface models: effects on photosynthesis and transpiration. In: *The Plant Journal* **101**.4, pp. 858–873.

Krinner, G. et al., (2005). A dynamic global vegetation model for studies of the coupled atmosphere-biosphere system: DVGM for coupled climate studies. In: *Global Biogeochemical Cycles* **19**.1, pp. 1–44.

Law, R.M., E.A. Kowalczyk, and Y.-P. Wang, (2006). Using atmospheric CO $_2$ data to assess a simplified carbon-climate simulation for the 20th century. In: *Tellus B: Chemical and Physical Meteorology* **58**.5, pp. 427–437.

Lawlor, David W. and A J Keys, (1993). Understanding photosynthetic adaptation to changing climate. In: *Plant adaptation to environmental stress*. London, United Kingdom: Chapman and Hall.

Leakey, A.D.B. et al., (2009). Elevated CO2 effects on plant carbon, nitrogen, and water relations: six important lessons from FACE. In: *Journal of Experimental Botany* **60**.10, pp. 2859–2876.

Lei, H. and D. Yang, (2010). Interannual and seasonal variability in evapotranspiration and energy partitioning over an irrigated cropland in the North China Plain. In: *Agricultural and Forest Meteorology* **150**.4, pp. 581–589.

Leuning, R., (1995). A critical appraisal of a combined stomatal-photosynthesis model for C3 plants. In: *Plant, Cell and Environment* **18**.4, pp. 339–355.

Leys, C. et al., (2013). Detecting outliers: Do not use standard deviation around the mean, use absolute deviation around the median. In: *Journal of Experimental Social Psychology* **49**.4, pp. 764–766.

Lloyd, J., (1991). Modelling Stomatal Responses to Environment in Macadamia integrifolia. In: *Australian Journal of Plant Physiology* **18**, pp. 649–660.

Lutaladio, N. and L. Castaldi, (2009). Potato: The hidden treasure. In: *Journal of Food Composition and Analysis* **22**.6, pp. 491–493.

MacKay, S.L. et al., (2012). The impact of induced drought on transpiration and growth in a temperate pine plantation forest. In: *Hydrological Processes*, p. 13.

Medlyn, B. E. et al., (2002). Temperature response of parameters of a biochemically based model of photosynthesis. II. A review of experimental data: Temperature response of photosynthetic parameters - review. In: *Plant, Cell & Environment* **25**.9, pp. 1167–1179.

Medlyn, B.E. et al., (2011). Reconciling the optimal and empirical approaches to modelling stomatal conductance. In: *Global Change Biology* **17**.6, pp. 2134–2144.

Migita, C., Y. Chiba, and T. Tange, (2007). Seasonal and spatial variations in leaf nitrogen content and resorption in a Quercus serrata canopy. In: *Tree Physiology* **27**.1, pp. 63–70.

Moorcroft, P.R., G.C. Hurtt, and S.W. Pacala, (2001). A method for scaling vegetation dynamics: The Excosystem Demography Model (ED). In: *Ecological Monographs* **71**.4, pp. 557–586.

NASA, (2021). *Global Climate Change Evidence: NASA Global Climate Change and Global Warming*. URL: `http://climate.nasa.gov/evidence/`. Accessed on 6th June 2021.

Obidiegwu, J.E., (2015). Coping with drought: stress and adaptive responses in potato and perspectives for improvement. In: *Frontiers in Plant Science* **6**.542, pp. 1–23.

Perdomo, J.A. et al., (2017). Rubisco and Rubisco Activase Play an Important Role in the Biochemical Limitations of Photosynthesis in Rice, Wheat, and Maize under High Temperature and Water Deficit. In: *Frontiers in Plant Science* **8**.490, pp. 1–15.

Reichstein, M. et al., (2002). Severe drought effects on ecosystem CO $_2$ and H $_2$ O fluxes at three Mediterranean evergreen sites: revision of current hypotheses? In: *Global Change Biology* **8**.10, pp. 999–1017.

Reichstein, M. et al., (2005a). Europe-wide reduction in primary productivity caused by the heat and drought in 2003. In: *Nature* **437**.7058, pp. 529–533.

Reichstein, M. et al., (2007). Reduction of ecosystem productivity and respiration during the European summer 2003 climate anomaly: a joint flux tower, remote sensing and modelling analysis. In: *Global Change Biology* **13**.3, pp. 634–651.

Reichstein, M. et al., (2013). Climate extremes and the carbon cycle. In: *Nature* **500**.7462, pp. 287–295.

Reichstein, Markus et al., (2005b). On the separation of net ecosystem exchange into assimilation and ecosystem respiration: review and improved algorithm. In: *Global Change Biology* **11**.9, pp. 1424–1439.

Rogers, A. et al., (2017). A roadmap for improving the representation of photosynthesis in Earth system models. In: *New Phytologist* **213**.1, pp. 22–42.

Sala, A. and J.D. Tenhunen, (1996). Simulations of canopy net photosynthesis and transpiration in Quercus ilex L. under the influence of seasonal drought. In: *Agricultural and Forest Meteorology* **78**.3, pp. 203–222.

Scoffoni, C. et al., (2012). Dynamics of leaf hydraulic conductance with water status: quantification and analysis of species differences under steady state. In: *Journal of Experimental Botany* **63**.2, pp. 643–658.

Sellers, P.J. et al., (1995). A Revised Land Surface Parametrization (SiB2) for Atmospheric GCMs. Part II: The Generation of Global Fields of Terrestrial Biophyscal Parameters from Satellite Data. In: *Journal of Climate* **9**, pp. 706–737.

Sinclair, T.R., L.C. Hammond, and J. Harrison, (1998). Extractable Soil Water and Transpiration Rate of Soybean on Sandy Soils. In: *Agronomy Journal* **90**.3, pp. 363–368.

Sitch, S. et al., (2003). Evaluation of ecosystem dynamics, plant geography and terrestrial carbon cycling in the LPJ dynamic global vegetation model. In: *Global Change Biology* **9**.2, pp. 161–185.

Sitch, S. et al., (2008). Evaluation of the terrestrial carbon cycle, future plant geography and climate-carbon cycle feedbacks using five Dynamic Global Vegetation Models (DGVMs): Uncertainty in land carbon cycle feedbacks. In: *Global Change Biology* **14**.9, pp. 2015–2039.

Smith, N.E. et al., (2020). Spring enhancement and summer reduction in carbon uptake during the 2018 drought in northwestern Europe. In: *Philosophical Transactions of the Royal Society B: Biological Sciences* **375**, pp. 1–11.

STATBEL, (2021). *Exploitations agricoles et horticoles*. URL: %5Curl%7Bhttps://statbel.fgov.be/fr/themes/agriculture-peche/exploitations-agricoles-et-horticoles#figures%7D. Accessed on 7th June 2021.

Tanner, C.B. and J.T. Ritchie, (1974). Evapotranspiration empiricisms and modelling. In: *American Society of Agronomy* **66**, pp. 1–15.

Terashima, I. and Y. Inoue, (1985). Vertical Gradient in Photosynthetic Properties of Spinach Chloroplasts Dependent on Intra-Leaf Light Environment. In: *Plant Cell Physiology* **26**.4, pp. 781–785.

Thom, A.S., (1972). Momentum, mass and heat exchange of vegetation. In: *Quarterly Journal of the Royal Meteorological Society* **98**.415, pp. 124–134.

Thomas, D.S. and D. Eamus, (1999). The influence of predawn leaf water potential on stomatal responses to atmospheric water content at constant Ci and on stem hydraulic conductance and foliar ABA concentrations. In: *Journal of Experimental Botany* **50**.331, pp. 243–251.

Tóth, B. et al., (2015). New generation of hydraulic pedotransfer functions for Europe: New hydraulic pedotransfer functions for Europe. In: *European Journal of Soil Science* **66**.1, pp. 226–238.

Trenberth, K.E. et al., (2014). Global warming and changes in drought. In: *Nature Climate Change* **4**.1, pp. 17–22.

Urban, Milan Oldřich et al., (2017). Proteomic and physiological approach reveals drought-induced changes in rapeseeds: Water-saver and water-spender strategy. In: *Journal of Proteomics* **152**, pp. 188–205.

Valentini, R. et al., (1995). In situ estimation of net CO2 assimilation, photosynthetic electron flow and photorespiration in Turkey oak (Q. cerris L.) leaves: diurnal cycles under different levels of water supply. In: *Plant, Cell and Environment* **18**.6, pp. 631–640.

Veihmeyer, F.J. and A.H. Hendrickson, (1931). The moisture equivalent as a measure of the field capacity of soils. In: *Soil science* **32**.3, pp. 181–193.

Vogel, E. et al., (2019). The effects of climate extremes on global agricultural yields. In: *Environmental Research Letters* **14**, pp. 1–13.

Vos, J. and J. Groenwold, (1989). Genetic differences in water-use efficiency, stomatal conductance and carbon isotope fractionation in potato. In: *Potato Research* **32**.2, pp. 113–121.

Vos, J. and P.J. Oyarzun, (1987). Photosynthesis and stomatai conductance of potato leaves – effects of leaf age, irradiance, and leaf water potential. In: *Photosynthesis Research* **11**, pp. 253–264.

Walker, A.P. et al., (2014). The relationship of leaf photosynthetic traits – Vcmax and Jmax – to leaf nitrogen, leaf phosphorus, and specific leaf area: a meta-analysis and modeling study. In: *Ecology and Evolution* **4**.16, pp. 3218–3235.

Wang, Y.-P. and R. Leuning, (1998). A two-leaf model for canopy conductance, photosynthesis and partitioning of available energy : Model description and comparison with a multi-layered model. In: *Agricultural and Forest Meteorology* **91**, pp. 89–111.

Watanabe, N., J.R. Evans, and W.S. Chow, (1994). Changes in the Photosynthetic Properties of Australian Wheat Cultivars Over the Last Century. In: *Functional Plant Biology* **21**.2, p. 169.

Weisz, R., J. Kaminski, and Z. Smilowitz, (1994). Water deficit effects on potato leaf growth and transpiration: Utilizing fraction extractable soil water for comparison with other crops. In: *American Potato Journal* **71**.12, pp. 829–840.

Wong, S.C., I.R. Cowan, and G.D. Farquhar, (1979). Stomatal conductance correlates with photosynthetic capacity. In: *Nature* **282**.5737, pp. 424–426.

Woodward, F.I. and M.R. Lomas, (2004). Vegetation dynamics – simulating responses to climatic change. In: *Biological Reviews* **79**.3, pp. 643–670.

Wutzler, Thomas et al., (2018). Basic and extensible post-processing of eddy covariance flux data with REddyProc. In: *Biogeosciences* **15**.16, pp. 5015–5030.

Xiao, Y., D. Tholen, and X.-G. Zhu, (2016). The influence of leaf anatomy on the internal light environment and photosynthetic electron transport rate: exploration with a new leaf ray tracing model. In: *Journal of Experimental Botany* **67**.21, pp. 6021–6035.

Zhou, S. et al., (2013). How should we model plant responses to drought? An analysis of stomatal and non-stomatal responses to water stress. In: *Agricultural and Forest Meteorology* **183**, pp. 204–214.